



RESEARCH ARTICLE

10.1029/2021JD036393

Key Points:

- Hourly PM₁₀ in China was estimated using interpretable deep forest and FY-4A top-of-the-atmosphere reflectance, and the daily and monthly mean R^2 were 0.82 and 0.97
- Excluding dust weather periods, the areas with high PM₁₀ values in China were mainly in cities and suburbs related to human activities
- The contribution of long-range transport dust and local pollution in China to PM₁₀ was both important during haze periods

Supporting Information:

Supporting Information may be found in the online version of this article.

Correspondence to:

B. Chen,
chenbin@lzu.edu.cn

Citation:

Bin, C., Song, Z., Huang, J., Zhang, P., Hu, X., Zhang, X., et al. (2022). Estimation of atmospheric PM₁₀ concentration in China using an interpretable deep learning model and top-of-the-atmosphere reflectance data from China's new generation geostationary meteorological satellite, FY-4A. *Journal of Geophysical Research: Atmospheres*, 127, e2021JD036393. <https://doi.org/10.1029/2021JD036393>

Received 23 DEC 2021
Accepted 10 APR 2022

Author Contributions:

Conceptualization: Bin Chen, Jianping Huang
Data curation: Zhihao Song, Peng Zhang, Xiuqing Hu, Xingying Zhang
Formal analysis: Zhihao Song
Investigation: Xiaodan Guan, Jiming Ge
Methodology: Bin Chen, Zhihao Song
Project Administration: Jianping Huang

© 2022. The Authors.

This is an open access article under the terms of the [Creative Commons Attribution License](#), which permits use, distribution and reproduction in any medium, provided the original work is properly cited.

Estimation of Atmospheric PM₁₀ Concentration in China Using an Interpretable Deep Learning Model and Top-of-the-Atmosphere Reflectance Data From China's New Generation Geostationary Meteorological Satellite, FY-4A

Bin Chen^{1,2} , Zhihao Song^{1,2}, Jianping Huang^{1,2} , Peng Zhang³, Xiuqing Hu³, Xingying Zhang³, Xiaodan Guan^{1,2} , Jiming Ge^{1,2} , and Xingzhao Zhou^{1,2}

¹Key Laboratory for Semi-Arid Climate Change of the Ministry of Education, College of Atmospheric Sciences, Lanzhou University, Lanzhou, China, ²Collaborative Innovation Center for Western Ecological Safety, Lanzhou, China, ³Key Laboratory of Radiometric Calibration and Validation for Environmental Satellites, National Satellite Meteorological Center, China Meteorological Administration, Beijing, China

Abstract The rapid urbanization in China and the long-range transport dust (LRTD) from arid and semi-arid areas has resulted in an increase of PM₁₀ concentration. In this study, an interpretable deep learning model [deep forest (DF)] with FY-4A top-of-the-atmosphere reflectance (TOAR) data were used to obtain the hourly PM₁₀ in China. The optimal hourly average R^2 of 10-fold cross validation can achieve 0.85 (13:00 Beijing time); The R^2 (RMSE, $\mu\text{g}/\text{m}^3$) of the daily, monthly, and annual averages were 0.82 (24.16), 0.97 (6.53), and 0.99 (2.30), respectively. Using TOAR data, the DF model performed better than other machine learning models. The feature importance of the TOAR-PM₁₀ model showed that TOAR and meteorological elements both contributed significantly to the model. In spring, the PM₁₀ in northern China was greater than that in southern China, which may be related to the LRTD. Excluding the dust weather periods, the areas with high PM₁₀ values in China were mainly in cities and their suburbs, where were correlated with human activities. During a dust weather process, LRTD increased PM₁₀ in northern China by 80.4%. During a mixture haze and dust weather process, the PM₁₀ increased by 130.2% in northern China, of which LRTD led to an increase of 73.7%. The sources (from the Taklimakan Desert in China) and transmission paths of these two LRTD processes were similar. The contribution of LRTD to PM₁₀ was related to dust intensity and meteorological conditions. The results showed that LRTD and local pollution to PM₁₀ was both important in haze periods.

1. Introduction

Atmospheric particulate matter with an aerodynamic diameter less than 10 μm (PM₁₀) has a great impact on global environmental (Jiang et al., 2015; Kassomenos et al., 2014; Millán-Martínez et al., 2021; Rastogi et al., 2020), human health (Brook et al., 2010; Ho et al., 2018; Samoli et al., 2011; Tomczak et al., 2016), and climate change (Q. Zhang et al., 2017; C. Zhao & Garrett, 2015). Since 2013, China has successively established more than 1,000 environmental monitoring stations to obtain the particle concentration (Yan et al., 2020; Q. Zhang et al., 2019; T. Zhang et al., 2019). However, because of the uneven spatial distribution of these ground stations, atmospheric PM₁₀ concentration data with continuous high spatial and temporal resolution are absent. This limits the research on the atmospheric PM₁₀ climate environment (Hu et al., 2014; Y. Zhang & Li, 2015).

Many scholars have obtained atmospheric particle matter concentrations with high spatio-temporal resolution by using machine learning models and satellite data (G. Chen et al., 2018; You et al., 2015; T. H. Zhang et al., 2016; Y. Zhang et al., 2021). Studies showed that there was a strong correlation between aerosol optical depth (AOD) and surface particles (Guo et al., 2009; Z. Li et al., 2016; Q. Xu et al., 2021), which is often used to estimate the particle concentration (Gui et al., 2020; T. Li et al., 2017; Xiong et al., 2021). Using the 5 km resolution AOD of the Medium Resolution Imaging Spectrometer (MERIS) sensor in three Malaysian metropolises and an artificial neural network to estimate PM₁₀ concentrations, the correlation coefficient of the model had values as large as 0.65 (Kanniah et al., 2014). The daily atmospheric PM₁₀ concentration in Israel was estimated based on the mixed effect model and MAIAC AOD, resulting a cross-validation, R^2 value of 0.79 (Kloog et al., 2015). Z. Zhang et al. (2018) used land-use regression (LUR) model to estimate the monthly PM10 concentration in China, and the R^2 reached 0.71. Based on random forest model and AOD data, G. Chen et al. (2018) successfully

Resources: Peng Zhang, Xiuqing Hu, Xingying Zhang
Software: Zhihao Song
Supervision: Jianping Huang, Xiaodan Guan, Jinming Ge
Visualization: Bin Chen, Zhihao Song
Writing – original draft: Bin Chen, Zhihao Song, Xingzhao Zhou
Writing – review & editing: Bin Chen, Jianping Huang

estimated the PM_{10} concentration in China in the past decade. Wei, Li, Xue, et al. (2021) used the space-time extremely randomized trees (STET) to generate PM_{10} data in China from 2015 to 2019, with a spatial resolution of 1 km, and pointed out that PM_{10} showed a significant downward trend. In addition, researchers have shown the relationship between AOD and particulate matter of polar orbiting satellites in China, such as MODIS (X. Wang et al., 2020), Visible Infrared Imaging Radiometer Suite (VIIRS; Wu et al., 2016), MISR (X. Meng et al., 2018), and Cloud-Aerosol Lidar with Orthogonal Polarization (CALIOP; Chen, Song, Pan, & Huang, 2022).

Polar orbiting satellites cannot obtain high time resolution data; however, the time resolution of second-generation geostationary satellites is ~ 15 min with a fine spatial resolution. Recently, some studies have begun to use geostationary satellites to obtain particle concentrations (W. Wang et al., 2017; Wei et al., 2019). Previously, the geostationary satellite AOD was principally used for $PM_{2.5}$ remote sensing (J. Liu et al., 2019; Z. Zhang et al., 2019). The inversion of PM_{10} was initiated in the 2 yr prior to this work. The geographically weighted region models and AOD of the Indian geostationary satellite (INSAT-3D) were used to estimate PM_{10} . The R^2 values of the pre-, post-, and winter models were 0.624, 0.718, and 0.633, respectively (Gupta et al., 2021). The AOD data from the Geostationary Ocean Color Imager (GOCI) of the Korean geostationary satellite (GEO-KOMPASAT 2B) was used to estimate the PM_{10} concentration based on two machine learning models [gradient boosted regression trees and light gradient boosting machine (LightGBM)]. The models achieved R^2 as high as 0.82 (S. Park et al., 2021). The hourly PM_{10} atmospheric concentrations in China were estimated using a deep learning algorithm and the AOD data from the Japanese geostationary satellite (Himawari-8). The hourly cross validation R^2 estimated by the AOD- PM_{10} model ranged from 0.82 to 0.88. The R^2 for daily, monthly, seasonal, and annual averages of atmospheric PM_{10} concentrations were 0.87, 0.91, 0.94, and 0.94, respectively (Chen, Song, Shi, & Li, 2022).

The particle concentration can be effectively estimated using the AOD (Stafoggia et al., 2019). Because AOD was only provided under optimal conditions, there were a large number of missing values (Y. Park et al., 2020). The coverage of satellite top-of-the-atmosphere reflectance (TOAR) was higher than that of AOD, so TOAR was used to directly obtain the particle concentration (L. Yang et al., 2020). Using the TOAR of Himawari-8 and the random forest model, the $PM_{2.5}$ of the Yangtze River Delta (YRD) in 2016 was obtained, and the 10-fold cross validation (R^2) was 0.75 (Bai et al., 2021). Using the TOAR of the Himawari-8 and LightGBM models, the R^2 of the $PM_{2.5}$ model was 0.86 (Yin et al., 2021). Using TOAR directly increases the effective coverage, and the performance of the model is also very positive.

Since the Himawari-8 satellite cannot cover Xinjiang, China (Song et al., 2021; Wei, Li, Pinker, et al., 2021), China's second-generation geostationary meteorological satellite FY-4A successfully launched on 11 December 2016, can cover the entire territory of China. Its Advanced Geosynchronous Radiation Imager (AGRI) imager can provide multi-band full-disk images with a time resolution of 15 min (Y. Chen et al., 2020; Mao et al., 2021; Zhang, Zhu, et al., 2019). As dust is an important component of PM_{10} , the Taklimakan Desert in Xinjiang, China is an important source of dust in East Asia. Using the FY-4A satellite was advantageous in estimating the contribution of dust weather to PM_{10} in East Asia (B. Chen et al., 2010). At the same time, there have been no studies on estimating PM_{10} from the FY-4A satellite. This study used the FY-4A satellite to estimate China's high spatial-temporal resolution for atmospheric PM_{10} concentrations.

Most studies have shown that nonlinear machine-learning models can more effectively obtain the particle concentration (Paschalidou et al., 2011; Qin et al., 2018; Yin et al., 2021). This study used a deep learning model, the deep forest (DF) model (Zhou & Feng, 2017), which has the structure of a deep neural network (DNN), and replaced DNN neurons with decision tree (DT) models. Combining the advantages of the DNN and DT models, the DF model can better fit nonlinear data and provide the importance of model features to result in a more interpretable deep learning model. The hourly PM_{10} concentrations in China from June 2018 to May 2019 were obtained using the DF model, FY-4A TOAR, meteorological parameters, and geographic information data. Using the results of the FY-4A TOAR- PM_{10} model, the contribution of long-range transport dust (LRTD) originating in the Taklimakan Desert to atmospheric PM_{10} concentrations in China and northern China was evaluated.

2. Data and Methods

2.1. FY-4A TOAR Data

FY-4A is China's second-generation geostationary meteorological satellite. It contains four advanced instruments: the AGRI, the Geosynchronous Interferometric Infrared Sounder, Lightning Mapping Imager, and Space

Table 1
Details of 14 Channels Information of the Advanced Geosynchronous Radiation Imager (AGRI) Instrument on FY-4A Satellite

Channel	Wavelength	Spatial resolution (km)	Main scientific objectives
1	0.45–0.49	1	Small particle aerosol, true color
2	0.55–0.75	0.5–1	Vegetation
3	0.75–0.90	1	Vegetation, aerosols
4	1.36–1.39	2	Cirrus cloud
5	1.58–1.64	2	Low cloud/snow identification, water cloud/ice cloud identification
6	2.1–2.35	2–4	Cirrus cloud, aerosol, particle size
7	3.5–4.0 (High)	2	Cloud and other high albedo targets, fire point
8	3.5–4.0 (Low)	4	Low albedo target, surface
9	5.8–6.7	4	Upper layer water vapor
10	6.9–7.3	4	Middle layer water vapor
11	8.0–9.0	4	Total water vapor and cloud
12	10.3–11.3	4	Cloud, surface temperature, etc.
13	11.5–12.5	4	Cloud, total water vapor, surface temperature
14	13.2–13.8	4	Cloud and water vapor

Environment Package; X. Zhang et al., 2020; Zhang, Lu, et al., 2019). The satellite provides high-precision data products for weather forecasting, environmental monitoring, climate change, and disaster prevention and reduction (C. Meng & Li, 2019; Min et al., 2017; Xia et al., 2020; J. Yang et al., 2017).

AGRI had 14 channels and a wavelength range of 0.45–13.8 μm . It covers the visible (VIS), near-infrared (NIR), medium infrared, and long infrared, with a spatial resolution of 0.5–4 km. As shown in Table 1, according to the scientific objectives of each spectral channel (channels related to the properties of aerosols), four channels related to particulate matter were selected to estimate PM_{10} , including 0.45–0.49 μm (VIS_B), 0.55–0.75 μm (VIS_G), 0.75–0.90 μm (VIS_R), and 2.1–2.35 μm (NIR). Cloud detection products (CLM) provided by the National Satellite Meteorological Center (NSMC) were used to remove the impact of clouds. For the TOAR data, mask processing was performed on the area where clouds or possible clouds were displayed in CLM. In this study, FY-4A Level 1 (L1) 4 km full disk dataset and CLM data with the same resolution obtained from NSMC from 1 June 2018 to 31 May 2019, were utilized.

2.2. PM_{10} Data and Auxiliary Data

The hourly atmospheric PM_{10} observation data were obtained from the China Environmental Monitoring Center (CEMC; China, 2012). Figure S1 in Supporting Information S1 showed the distribution of the 1,641 CEMC ground PM_{10} stations. The box in the figure shows six typical urban agglomerations in China: the Guanzhong Plain (GZP), Pearl River Delta (PRD), Central China (CC), Beijing-Tianjin-Hebei (BTH), Sichuan Basin (SCB), and Yangtze River Delta (YRD).

Auxiliary data include meteorological parameters, geographic information, and time variables. Previous studies have shown that meteorological parameters and geographic information have an impact on pollutant transmission and accumulation of pollutants (Fu et al., 2008; Gao et al., 2016; Sun et al., 2016). Meteorological parameters include boundary layer height (BLH, m; Han et al., 2018), 2 m air temperature (TM, K; Ma et al., 2021), relative humidity (RH, %; F. Liu et al., 2019), u and v components of 10 m wind (U_{10} , V_{10} , m/s; B. Xu et al., 2020), and surface air pressure (SP, Pa; G. Xu et al., 2020). These data were obtained from ERA-5 ECMWF reanalysis data (<https://cds.climate.copernicus.eu/cdsapp#!/dataset/reanalysis-era5-land>). The temporal resolution of per hour and a spatial resolution of $0.25^\circ \times 0.25^\circ$ or $0.1^\circ \times 0.1^\circ$ (Table 2 for more details). Geographic information, including ECMWF's high and low vegetation index (LL, LH), NASA's height (HEIGHT), and population density (PD; M. Chen et al., 2020), were obtained from NASA's socio-economic data and Applications Center (SEDAC).

Table 2
Model Validation Results for Six Large Urban Agglomerations

Area	R^2	RMSE ($\mu\text{g}/\text{m}^3$)	MAE ($\mu\text{g}/\text{m}^3$)	N
Beijing-Tianjin-Hebei	0.86	22.04	13.57	58,857
Guanzhong Plain	0.85	22.29	13.78	36,714
Centra China	0.87	18.05	11.96	128,167
Sichuan Basin	0.81	15.08	10.44	49,801
Pearl River Delta	0.80	13.73	9.44	48,263
Yangtze River Delta	0.86	15.70	10.69	155,458

The time variable (TIME) refers to the hour difference between the current time and 0:00 on 1 January 1900. The data used in the model are listed in Table S1 in Supporting Information S1.

2.3. Deep Forest Model

Zhou and Feng (2017) proposed the DF model, which uses an extreme tree (ET; Geurts et al., 2006) and random forest (RF; Breiman, 2001) as neurons of the model, and multiple neurons formed a hidden layer. The DF model includes N hidden layers, and the output of the last hidden layer is connected to a separate estimator LightGBM (Ke et al., 2017) to output the results of the model. Because the DF model neurons were tree models (such as RF and ET), the DF model can output the importance of features, which makes the

DF model interpretable. In this study, a DF model with three hidden layers was designed. Each layer contained 12 neurons (6 ETs and 6 RFs). Figure 1 is a structural diagram of the PM_{10} concentration obtained by the DF model.

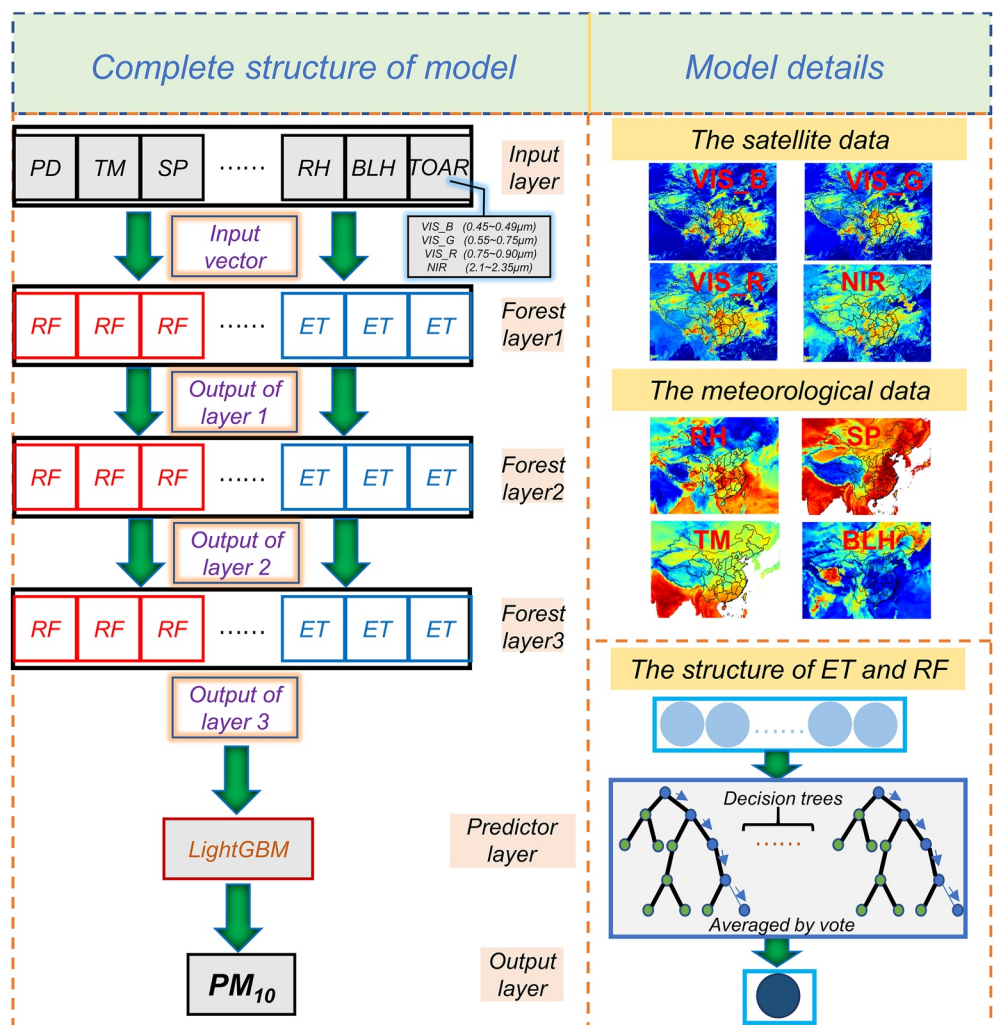


Figure 1. The schematic diagram of estimating PM_{10} using FY-4A TOAR data and deep forest (DF) model. The upper part of the right column is the distribution of input features, such as VIS_B, VIS_G, VIS_R, NIR, RH, SP, TM, and BLH on 28 April 2019, 12:00 (Beijing Time), and the lower part of the right column is the structure of the neuron [extreme tree (ET) and random forest (RF)].

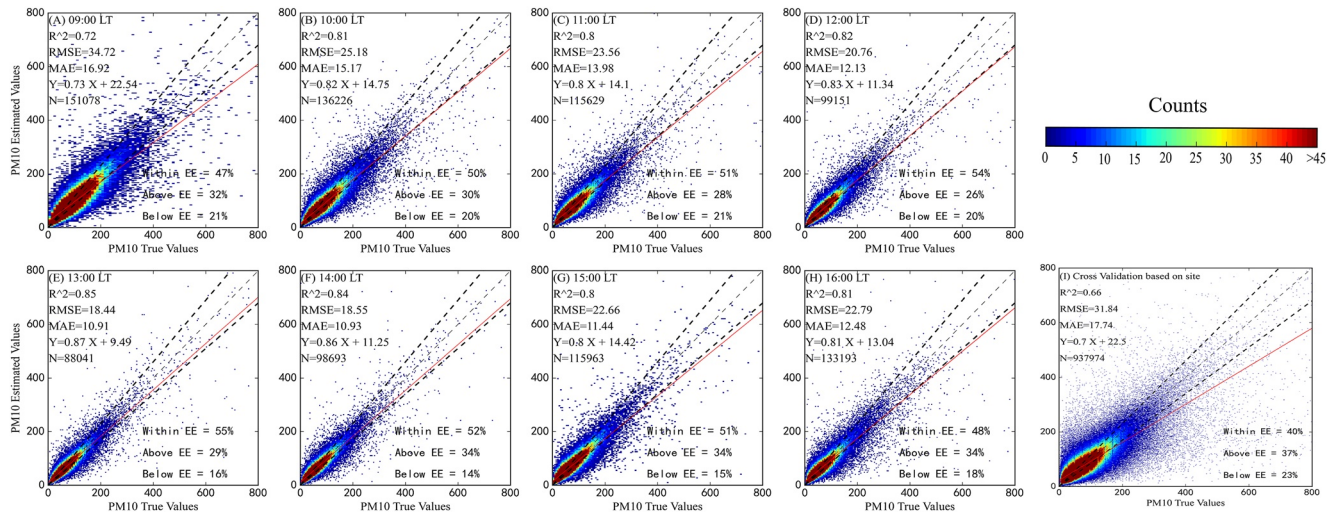


Figure 2. Hourly cross validation results of FY-4A TOAR-PM10 model based on grid points, and (a–h) is 9:00–16:00 Beijing time respectively. (I) represents hourly cross validation results based on sites. The dark dotted line represents the error line, the light dotted line represents the 1:1 line, and the solid red line represents the linear regression fitting line, EE presents the expected error, when the ratio of the estimated value to the true value is between 1.15 and 0.85. The discrepancy between them is called EE.

2.4. Data Preprocessing

The spatial resolution of meteorological elements and geographic information was adjusted to $0.04^\circ \times 0.04^\circ$ of FY-4A data by bilinear interpolation. The PM_{10} hourly mean data of CEMC were compared with those of the TOAR of FY-4A. After data matching, the total number of samples was 937,974, of which the number of samples in spring (MAM), summer (JJA), autumn (SON), and winter (DJF) were 229,769, 259,037, 300,717, and 148,451, respectively.

2.5. Model Validation

A 10-fold cross-validation method was used to test the model performance (Rodriguez et al., 2010). The parameters used to describe the model performance included the determination coefficient (R^2), root mean square error (RMSE), and mean absolute error (MAE; Chen, Song, Pan, & Huang, 2022; Chen, Song, Shi, & Li, 2022). The expected error (EE, Equation 1) was used to evaluate the accuracy of the TOAR- PM_{10} model. The better EE value (close to 100%) indicated that the estimated value of the model is agree with the observation value (Chu et al., 2003; X. Yang et al., 2020).

$$EE = (1 \pm 0.15)y_i \pm 0.05 \quad (1)$$

y_i represents the observed value of PM_{10} from CEMC.

3. Model Validation Results

3.1. Time Scale Results (Hourly, Daily, Monthly, Seasonal, and Annual Mean)

The TOAR- PM_{10} model was established using the DF model, and the estimated atmospheric PM_{10} concentration values were compared with the observed values of the CEMC. The results were shown in Figure 2. Except at 09:00 a.m. Beijing time, the 10-fold cross validation R^2 was greater than 0.8. At 13:00, the R^2 value of the model reached a maximum of 0.85, and 55% of the samples fell within EE. The fitting slope comparing the estimated value and the observed value was >0.8 , indicating that the TOAR- PM_{10} model estimated most atmospheric PM_{10} samples well, and the estimated value was consistent with the observed value. The RMSE of the model was 18.44–34.72 $\mu\text{g}/\text{m}^3$ with a MAE is 10.91–16.92 $\mu\text{g}/\text{m}^3$. This showed that it was feasible to directly obtain PM_{10} concentration data using FY-4A TOAR data, and the model performance was mainly related to pollutant

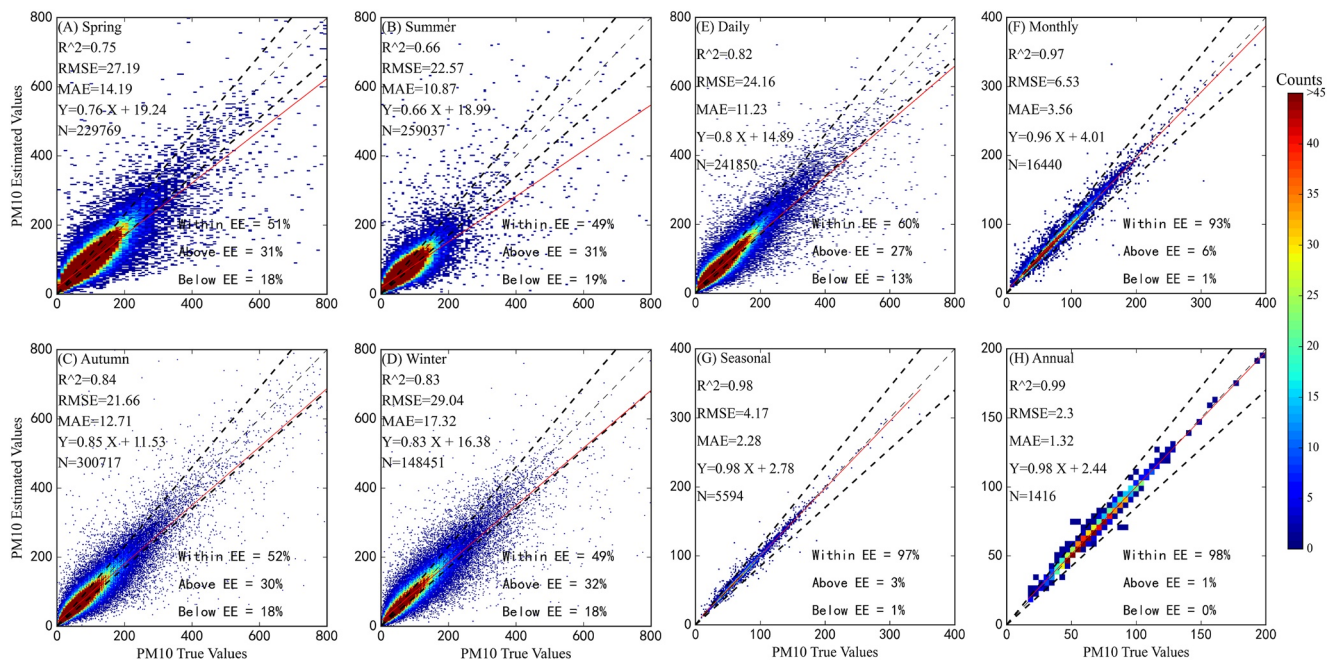


Figure 3. Similar to Figure 2, except for spring (a), summer (b), autumn (c), winter (d), daily (e), monthly (f), seasonal (g), and annual (h) average cross validation results of FY-4A TOAR-PM₁₀ model based on grid points.

emissions and meteorological conditions (J. Chen et al., 2019; Zang et al., 2019; C. Zhao et al., 2020). As shown in Figure 2 (I), the R^2 of the out-of-station cross validation results was 0.66, which was worse than the data based on grid points. This was because some stations did not participate in the training data of the model, so that the model could not obtain the effective information of the region. In general, considering the overall performance of the model, the DF model could effectively estimate the PM₁₀ concentration in the area without sites.

As shown in Figures 3a–3d, the TOAR-PM₁₀ estimation model performed best in autumn with a cross validation R^2 was 0.84 (RMSE was 21.66 $\mu\text{g}/\text{m}^3$). Performance was poor during summer R^2 with a value of only 0.66 (RMSE was 22.57 $\mu\text{g}/\text{m}^3$). R^2 in spring and winter were 0.75 and 0.83, respectively; however, RMSE in these two seasons was relatively high, 27.19 and 29.04 $\mu\text{g}/\text{m}^3$, respectively. This may be related to the frequent occurrence of dust weather in spring and the large combustion of fossil fuels for heating in winter (Xiao et al., 2015; Y. Yang et al., 2016). In addition, the estimated atmospheric PM₁₀ concentrations was compared with station observations on daily, monthly, seasonal, and annual average PM₁₀. The results were shown in Figures 3e–3h. The daily, monthly, seasonal, and annual validation results R^2 (RMSE) of TOAR-PM₁₀ model were 0.82 (24.16 $\mu\text{g}/\text{m}^3$), 0.97 (6.53 $\mu\text{g}/\text{m}^3$), 0.98 (4.17 $\mu\text{g}/\text{m}^3$), and 0.99 (2.30 $\mu\text{g}/\text{m}^3$), respectively. The results showed that the PM₁₀ estimated using the TOAR-PM₁₀ model was reliable.

3.2. Spatial Scale Results

Figure 4 showed the spatial performance of the TOAR-PM₁₀ model. In most stations in eastern China, model R^2 was relatively high (>0.8), while in western China, the model performance was degraded, especially in the Qinghai Tibet Plateau, which has very complex terrain. There was a large difference in the number of stations in eastern and western China. The model performed relatively well in areas with large samples, and R^2 showed a high distribution in eastern China and low distribution in western China. The distribution of RMSE and MAE in China was high in the North and low in the South, especially in Northwest China, and RMSE and MAE were greater than 18 and 24 $\mu\text{g}/\text{m}^3$, respectively. The validation results of the six typical urban agglomerations in China were shown in Table 2. The Yangtze River Delta, Beijing Tianjin Hebei and Central China demonstrated good model performance, with R^2 (RMSE) of 0.86 (15.70 $\mu\text{g}/\text{m}^3$), 0.86 (22.04 $\mu\text{g}/\text{m}^3$), and 0.87 (18.05 $\mu\text{g}/\text{m}^3$), respectively. The R^2 values in the Sichuan Basin and Pearl River Delta were less than 0.82. R^2 performed well, mainly

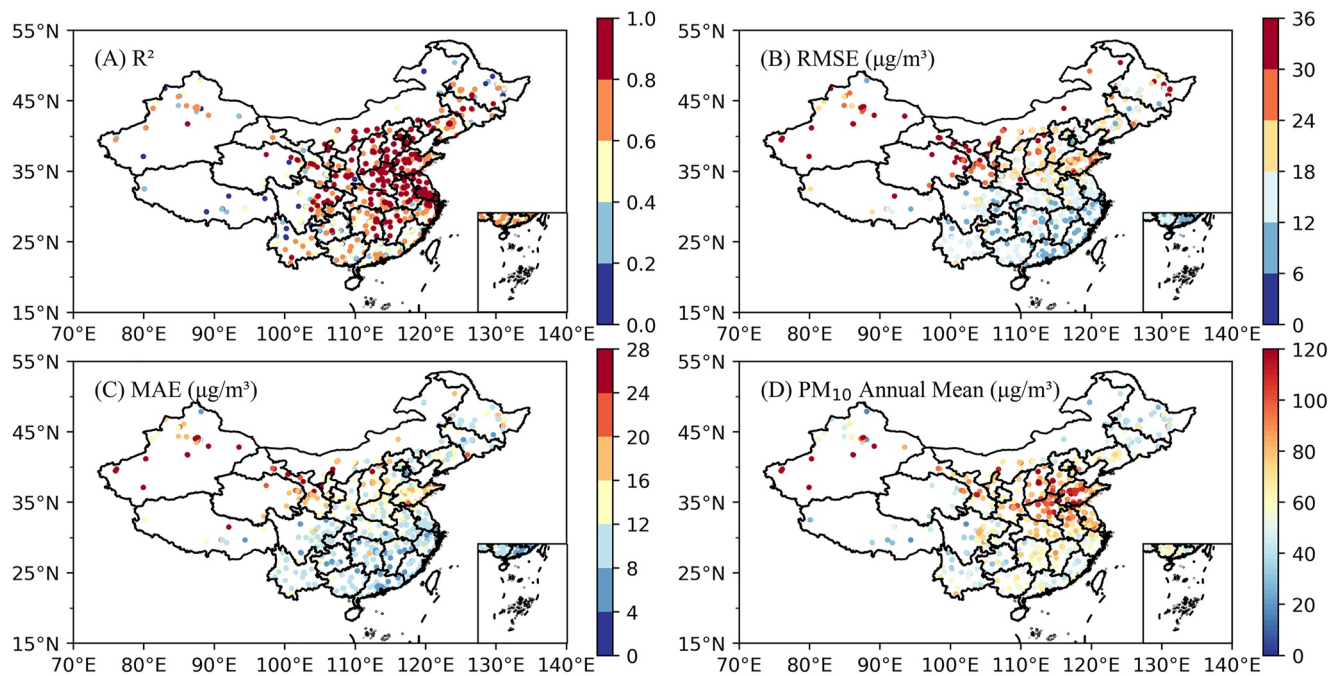


Figure 4. Spatial distribution of FY-4A TOAR-PM₁₀ model evaluation indicators, (a: R^2 , b: RMSE, c: MAE, and d: PM₁₀ annual mean.)

in urban agglomeration areas, and performed poorly, mainly in areas with complex topographic conditions, such as the western Sichuan Basin.

3.3. Importance of Model Features

The deep learning DNN model is a “black box,” which cannot provide interpretability to the model. The neuron of the deep learning DF model is a tree model, which can obtain the importance of model features and the contribution of model input variables. To evaluate the importance of each input feature in different seasons (or regions), we used the same DF architecture (as described in Section 2.3) and retrained the data in seasons (or regions) to obtain the feature importance. Except for Figure 5a (spring, summer, autumn, and winter) and Figure 5b, the other results of the model in this article were the results of the same TOAR-PM₁₀ model constructed based on the whole sample, such as Figure 5a (Annual).

As shown in Figure 5a, the feature importance of TOAR (the sum of the feature importance of the four channels) was the highest, followed by the TIME variable. Among the meteorological elements, BLH, RH, and TM made significant contributions to the model. In addition, a low vegetation index (LL) also affected the performance of the model. Generally speaking, the feature importance of each input was different in seasons, but in the season with poor model performance, the contribution of other importance features was low except for TOAR. Figure 6 showed the variation trend of uncertainty (RMSE) with important features. The results indicate that the uncertainty of derived PM₁₀ varies with TOAR and meteorological elements. In general, various factors (including TOA and meteorological factors) influence the uncertainty of derived PM₁₀. RMSE decreased with the increase of VIS_B, VIS_G, VIS_R, BLH, and TM. The effect of NIR and RH on RMSE was about 20 μg/m³. Furthermore, based on the feature importance, the main influencing factors of each region will change. In addition, we performed linear fitting for each estimation factor and model bias, and the regression coefficient obtained is shown in Figure S2 in Supporting Information S1. The results indicated that the factors such as VIS_G, VIS_R, RH, LL, SP, TM, and height contributed more (absolute value of the regression coefficient >1) to the uncertainty of the estimation results.

In addition, as shown in Figure 5b, the feature importance of TOAR in each region was ~0.15, while meteorological elements, geographic information, and time variables changed significantly. BLH and RH had a significant impact on the BTH region, but their contributions to other regions were relatively low. The contribution of TM to

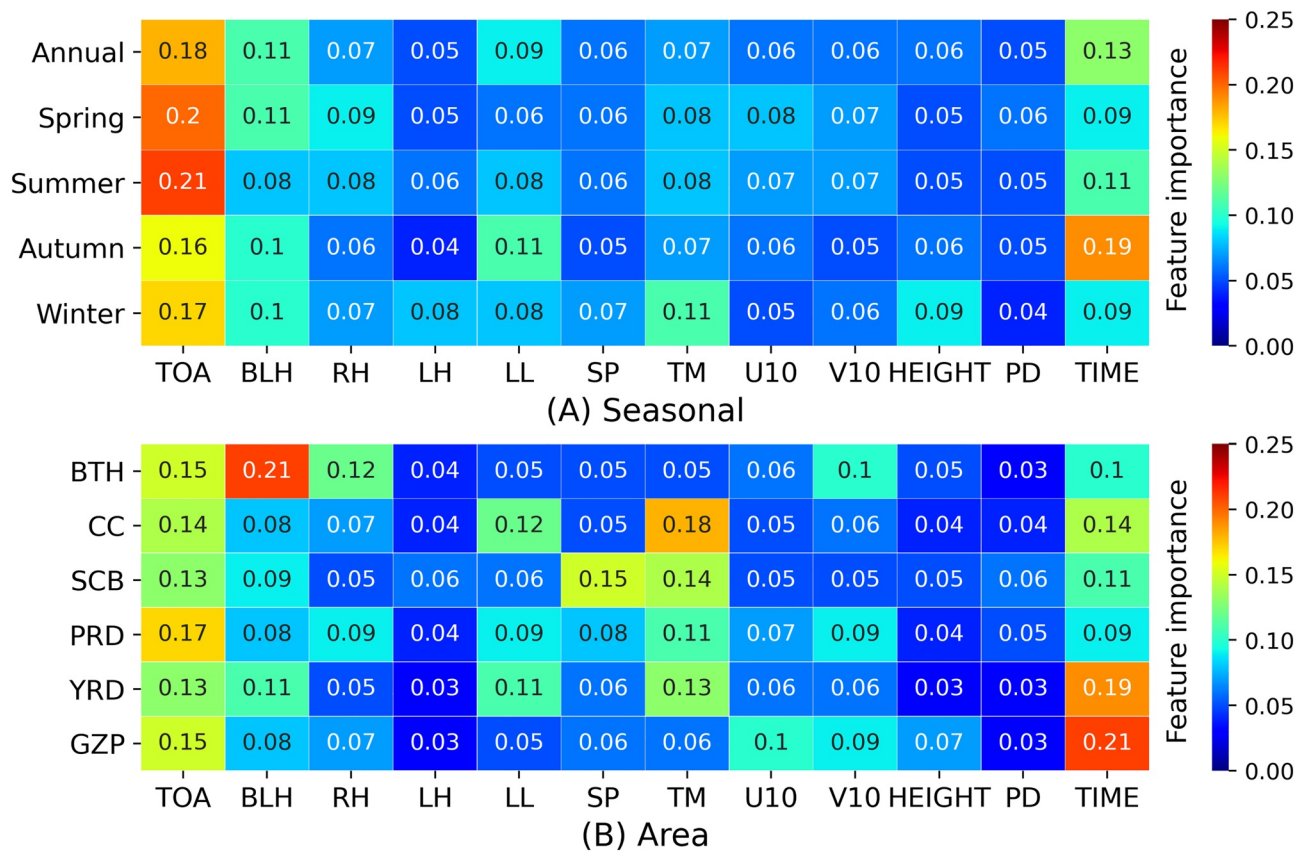


Figure 5. The feature importance of DF in (a) annual and seasons and (b) six urban agglomerations. The color and number of each grid point on the panel represent the feature importance score in the DF model.

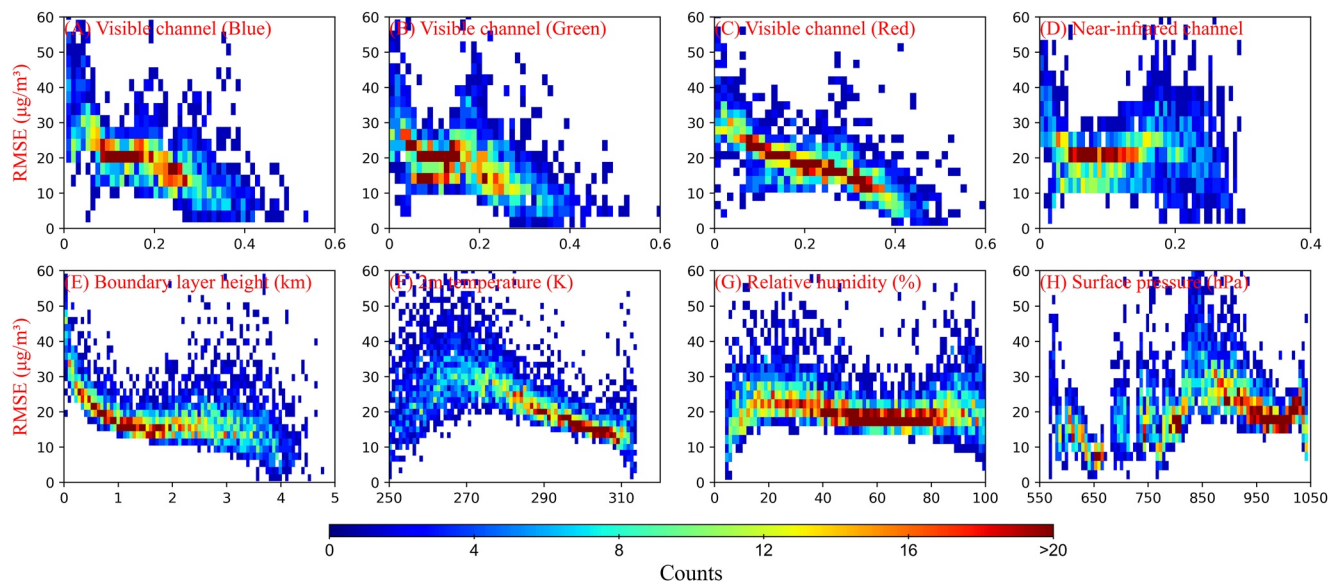


Figure 6. The variation trend of RMSE with important features and color bar indicates the number of points.

CC, SCB, PRD, and YRD exceeded 0.1. The importance of SP was only >0.1 in the SCB area with poor model performance. For the YRD and GZP regions, the TIME variable was a very important variable. The dominant features of the model would change in different seasons and regions, which also explained why the out-of-station cross validation result of the model was relatively poor, as shown in Figure 2 (I).

4. PM₁₀ Distribution Results

4.1. Spatial Distribution of Hourly and Seasonal Average for Atmospheric PM₁₀ Concentrations

The average PM₁₀ concentration distribution from 09:00 to 16:00 Beijing during the study period was shown in Figure 7. The estimation results of TOAR-PM₁₀ showed that the Tarim Basin had the highest concentration of atmospheric PM₁₀ concentration in China, with a daily average concentration of 100 $\mu\text{g}/\text{m}^3$, which is correlated with frequent local dust aerosols. The concentration of PM₁₀ in BTH region showed obvious diurnal variation: it was the greatest from 09:00 to 10:00 ($73.15 \pm 22.81 \mu\text{g}/\text{m}^3$), then decreased to $56.22 \pm 9.87 \mu\text{g}/\text{m}^3$ at 13:00. At 16:00 it increased slightly ($63.03 \pm 13.71 \mu\text{g}/\text{m}^3$). The PM₁₀ concentration in GZP had the same diurnal variation as that in the BTH area ($61.10 \pm 19.96 \mu\text{g}/\text{m}^3$, $55.87 \pm 10.98 \mu\text{g}/\text{m}^3$, and $58.01 \pm 12.53 \mu\text{g}/\text{m}^3$). The concentration of PM₁₀ in southern China continued to decline from 09:00 to 16:00, but there were great differences among regions: the concentration of PM₁₀ in the YRD region was 65 $\mu\text{g}/\text{m}^3$ and greater; The hourly variation range of PM₁₀ concentration in CC region was $60.38 \pm 17.53 \mu\text{g}/\text{m}^3$; The hourly PM₁₀ of SCB region was $53.22 \pm 11.25 \mu\text{g}/\text{m}^3$; The concentration of atmospheric PM₁₀ in the YRD region was less than 50 $\mu\text{g}/\text{m}^3$. In addition, the concentration of PM₁₀ in other parts of China was relatively low, especially in Northeast China and the Qinghai Tibet Plateau. The results indicated that the estimated results were in good agreement with the observed results.

As shown in Figure S3 in Supporting Information S1, the average atmospheric PM₁₀ concentration values during the four seasons in China were 67.90 ± 25.78 , 49.8 ± 20.06 , 58.68 ± 22.16 , and $73.46 \pm 26.27 \mu\text{g}/\text{m}^3$, respectively. Because of the frequent dust weather in spring, the atmospheric PM₁₀ concentration in the Tarim Basin, one of the dust sources in East Asia, was very high, and the PM₁₀ concentration in North China was generally greater than that in South China. In winter, due to low wind speeds, meteorological conditions were not conducive to pollutant diffusion. Winter is the heating season in northern China. The PM₁₀ concentrations in the BTH, GZP, YRD, and SCB regions were greater in winter. Compared with those of winter, the anthropogenic emissions in summer and autumn were lower. In addition, there was more precipitation during summer and autumn resulting in a moisture-based elimination, wet deposition, of atmospheric PM₁₀. This elimination resulted in a lower atmospheric PM₁₀ concentration during summer and autumn.

4.2. PM₁₀ Distribution of Six Large Urban Agglomerations in China

The spatial resolution of the TOAR data provided by FY-4A was 4 km, which reflected the atmospheric PM₁₀ concentration distribution at the city level. Figure 8 showed the annual average atmospheric PM₁₀ concentration distribution of six large urban agglomerations in China. The results showed that the concentration of atmospheric PM₁₀ was higher in BTH ($66.66 \pm 16.92 \mu\text{g}/\text{m}^3$), CC ($64.22 \pm 14.78 \mu\text{g}/\text{m}^3$), and YRD ($79.34 \pm 15.86 \mu\text{g}/\text{m}^3$) region. The concentration of atmospheric PM₁₀ in GZP and SCB was relatively low, $\sim 59.05 \pm 14.71 \mu\text{g}/\text{m}^3$. The annual atmospheric concentration of PM₁₀ in the PRD region was only $49.76 \pm 6.53 \mu\text{g}/\text{m}^3$. According to the distribution of atmospheric PM₁₀, areas of high atmospheric PM₁₀ concentrations in each region generally occurred in large cities and surrounding areas, which were closely related to local human activities.

4.3. Case 1: Contribution of Long-Range Transport Dust to Atmospheric PM₁₀ Concentration

From 14 to 17 May 2019, a large-scale dust storm occurred in northern China (35°N – 45°N , 70°E – 135°E). Combined with the spaceborne lidar CALIOP data, the results of the TOAR-PM₁₀ model were used to analyze the dust weather process. Figure 9 (Part 1) showed the three-dimensional transmission diagram of CALIOP's observational data of the dust weather process. The red transmission line was the forward trajectory line of the HYSPLIT mode. It can be observed that the dust weather originated in Taklimakan desert of China, traversed northern China to the Yellow Sea on May 17.

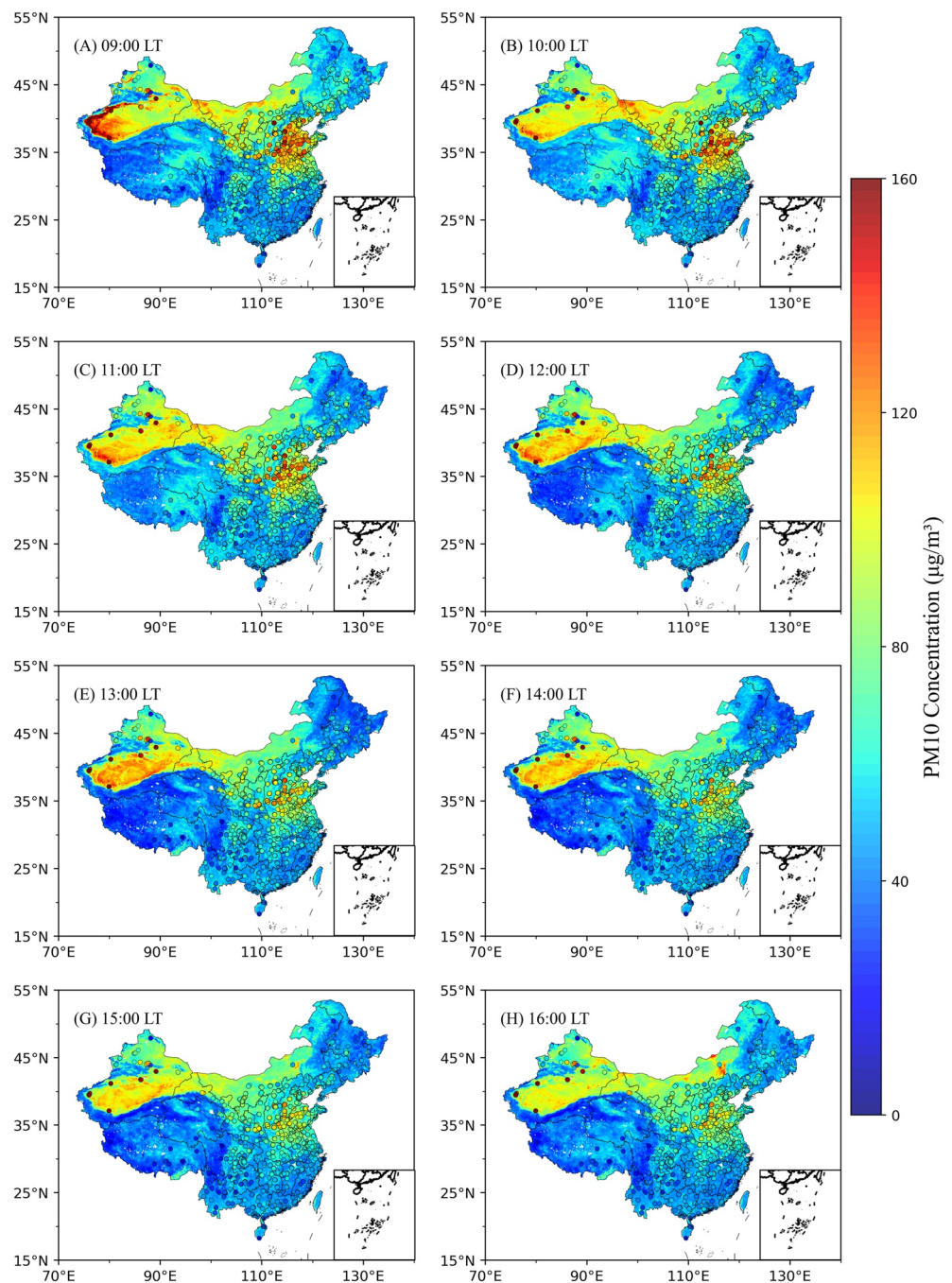


Figure 7. Diurnal variation of PM_{10} concentration in China using FY-4A TOAR- PM_{10} model. (a–h) represents the PM_{10} concentrations between 09:00 and 16:00 Beijing time. These points represent PM_{10} concentrations observed at ground stations from CEMC.

Figure S4 in Supporting Information S1 showed the cloud and aerosol profiles obtained by CALIOP during this dust weather process. The dust aerosol ascended to an altitude greater than 8 km; consequently, it could be transmitted downstream for long distances. There was a wide range of dust aerosols at an altitude of 0–8 km in northern China, and on the 17th, there was a large area of polluted continental aerosols and polluted dust aerosols in the southern Yellow Sea. The red line in Figure 10 was the orbit of CALIOP, and the left column was the FY-4A true color map. There were many white clouds in the map, which resulted in the vacancy value of the estimated atmospheric PM_{10} concentration. It can also be seen from the figure that there was a large quantities of dust

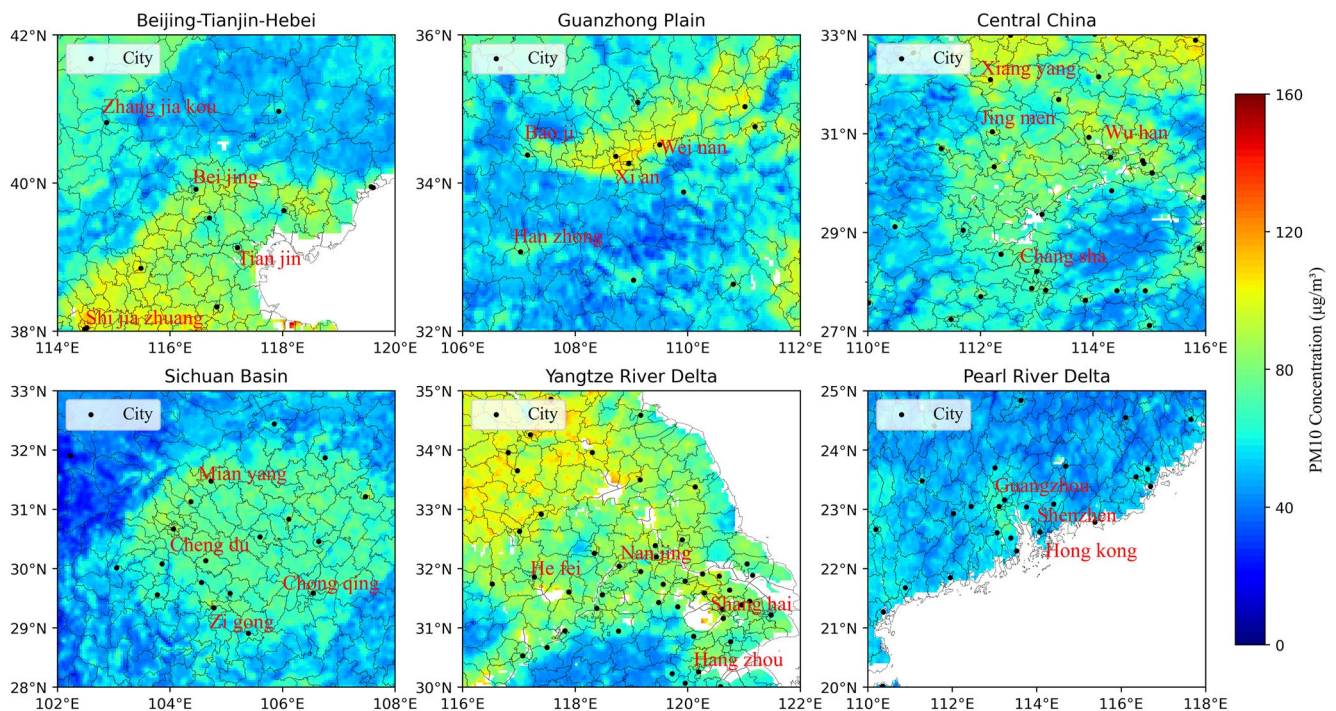


Figure 8. Distribution of atmospheric PM_{10} concentration in the six large urban agglomerations in China. Black dots represent cities, and some big cities were shown in red. Each region name was displayed on the submap title.

aerosols in northern China (earthy yellow). Station observations (Figure 10, middle column) and model estimation (Figure 10, right column) showed that the atmospheric PM_{10} concentration first increased and then decreased from the 14th to 17th. From 14 to 17 May 2019, the estimated values of atmospheric PM_{10} concentrations in China were 98.53, 91.02, 99.95, and 77.22 $\mu\text{g}/\text{m}^3$ (northern China: 123.82, 121.98, 139.77, and 106.90 $\mu\text{g}/\text{m}^3$). The observed values of PM_{10} concentration stations were 102.81, 96.00, 91.88, and 60.90 $\mu\text{g}/\text{m}^3$ (northern China: 134.49, 169.54, 130.04, and 77.86 $\mu\text{g}/\text{m}^3$). Figure S5 in Supporting Information S1 showed the 10 m wind field during dust weather, and PM_{10} was the estimated value of the TOAR- PM_{10} model. The wind speed in northern China was significantly greater than that in southern China. The surface wind in northern China was generally westerly. The area with high surface wind speed corresponded to the high atmospheric PM_{10} concentration and dust transmission path.

As shown in Figure 9 (Part 2), it was the atmospheric PM_{10} concentration (Figure 9a, Dust period) during the dust weather process (14–17 May 2019) and the atmospheric PM_{10} concentration (Figure 9b, None_Dust period) without dust weather in May 2019. In addition, the difference (Figure 9c, Dust period—None_Dust period) between the two periods was presented. The left column was the station observation value, and the right column was the estimated value of TOAR- PM_{10} model, and through the difference (Figure 9c), we can estimate the contribution of LRTD to atmospheric PM_{10} concentration during dust weather. During this dust weather process (Dust Period), the estimated and observed atmospheric PM_{10} concentrations in China were 87.53 and 87.78 $\mu\text{g}/\text{m}^3$, respectively (northern China: 116.64 and 127.96 $\mu\text{g}/\text{m}^3$). The estimated and observed atmospheric PM_{10} concentration values in None_Dust period in May 2019 were 57.46 and 55.49 $\mu\text{g}/\text{m}^3$, respectively (northern China: 64.64 and 64.91 $\mu\text{g}/\text{m}^3$). Based on the model results, during the dust weather, the atmospheric PM_{10} concentration in 64% of China's regions increased by 20%. In 39% of China's regions, it increased by 50%. In 28% of China's regions, it increased by 70%. Finally, 17% of China's regions it increased by 100%. Based on the CEMC stations, the atmospheric PM_{10} concentration at 827 stations (accounting for 52% of the total stations) increased by 20%. At 592 stations (37%), it increased by 50%. At 484 stations (30%), it increased by 70%. Finally, at 379 stations (23%), it increased by 100%. The model estimates were consistent with station observations for atmospheric PM_{10} concentrations.

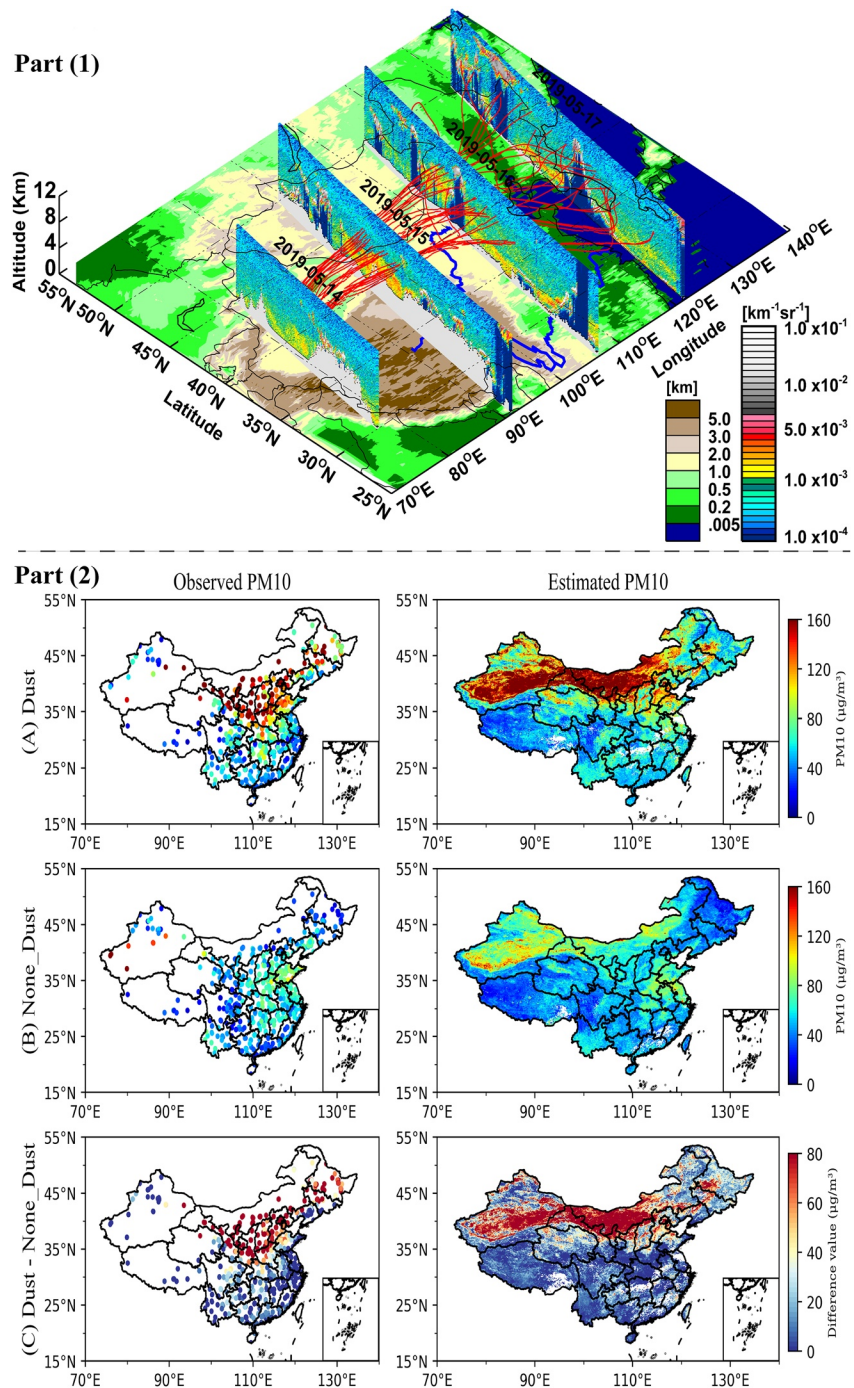


Figure 9. Part (1) showed dust weather event (14–17 May 2019), red lines represented back trajectory analyses and dust transport. Vertical images (curtain files) showed the CALIPSO 532-nm total attenuated backscatter. The color scales on the left represent topographical elevation, and the color scales on the right represent 532-nm total attenuated backscatter. Part (2) showed the distribution of atmospheric PM_{10} concentration estimated by the model (left column) and observed by the station (right column). Figure line (a), (b), and (c) showed the average atmospheric PM_{10} concentration of Dust period, None_Dust period, and the difference between Dust period and None_Dust period, respectively.

4.4. Case 2: Changes in PM_{10} Concentration Under the Combined Conditions of Dust and Haze Weather

On 24–30 November 2018, there was a large area of haze in China. In addition, there was an LRTD weather process in northern China on November 25–27 (the largest area of dust on November 26). This event was a

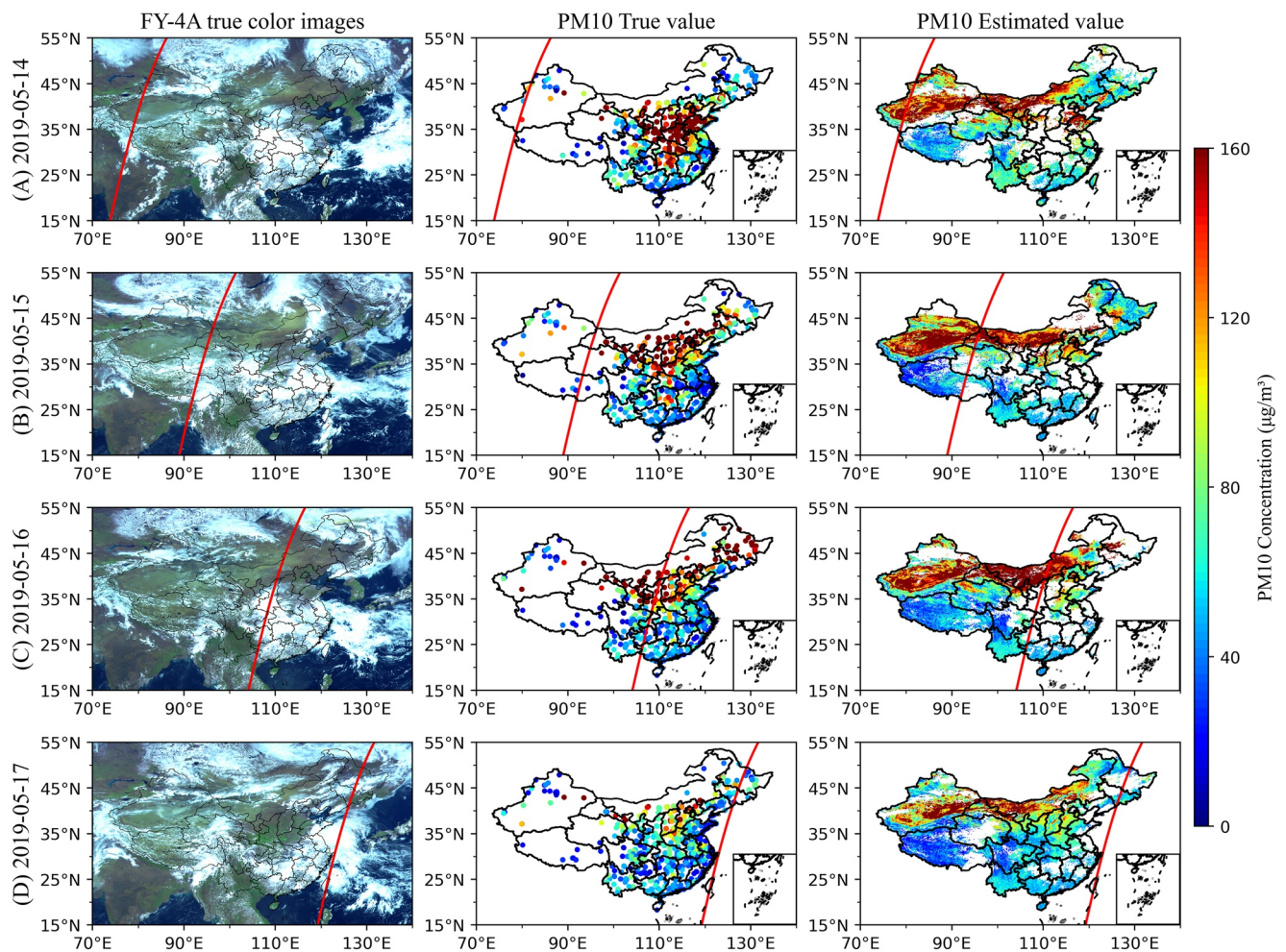


Figure 10. The same as Figure 9 (Part 2), except that the left column was the true color map of FY-4A satellite, the middle column was the daily average PM_{10} obtained by the CEMC stations, the right column was the daily average PM_{10} estimated by the TOAR- PM_{10} model, and the red solid line was the CALIOP orbit. Line (a): 5–14, Line (b): 5–15, Line (c): 5–16, and Line (d): 5–17 for 2019.

composite pollution weather event of dust and haze weather. The haze period was November 24–30 (haze period), the dust weather period was November 25–27 (dust period), and the period of no dust nor haze weather was November 1–23 (None_Haze_Dust period). As shown in Figure 11 (Part 1), CALIOP observed the three-dimensional transmission of the dust weather process. The source and transmission path of the dust weather were similar to the dust weather process in May 2019 (as shown in Figure 9, Part 1), but the dust intensity and transmission height were less.

In Figure S6 in Supporting Information S1, a large area of dust aerosols and pollution dust aerosols were found at an altitude of 0–4 km in China from the 24th to 27th, and a small amount of dust aerosol was found at an altitude of 8 km on the 26th, which also showed that the dust intensity was less. The FY-4A true color (RGB) map in Figure 12 showed clouds (white), which was consistent with the observation of CALIOP (Figure S6 in Supporting Information S1). From 24 to 27 November 2018, the estimated atmospheric PM_{10} concentrations in China were 81.98, 95.23, 198.47, and 142.84 $\mu\text{g}/\text{m}^3$ (northern China: 101.32, 107.38, 292.72, and 207.59 $\mu\text{g}/\text{m}^3$), and the observed atmospheric PM_{10} concentrations were 99.32, 130.18, 174.98, and 171.59 $\mu\text{g}/\text{m}^3$ (northern China: 122.50, 193.56, 302.76, and 276.10 $\mu\text{g}/\text{m}^3$). The difference between the estimated and observed values was due to the missing values of the estimated PM_{10} caused by cloud cover. Figure S7 in Supporting Information S1 showed the wind field of the dust-weather process. The wind speed was low in the southern region and high in the northern region of China. The wind speed was greatest on November 26, which was also consistent with the

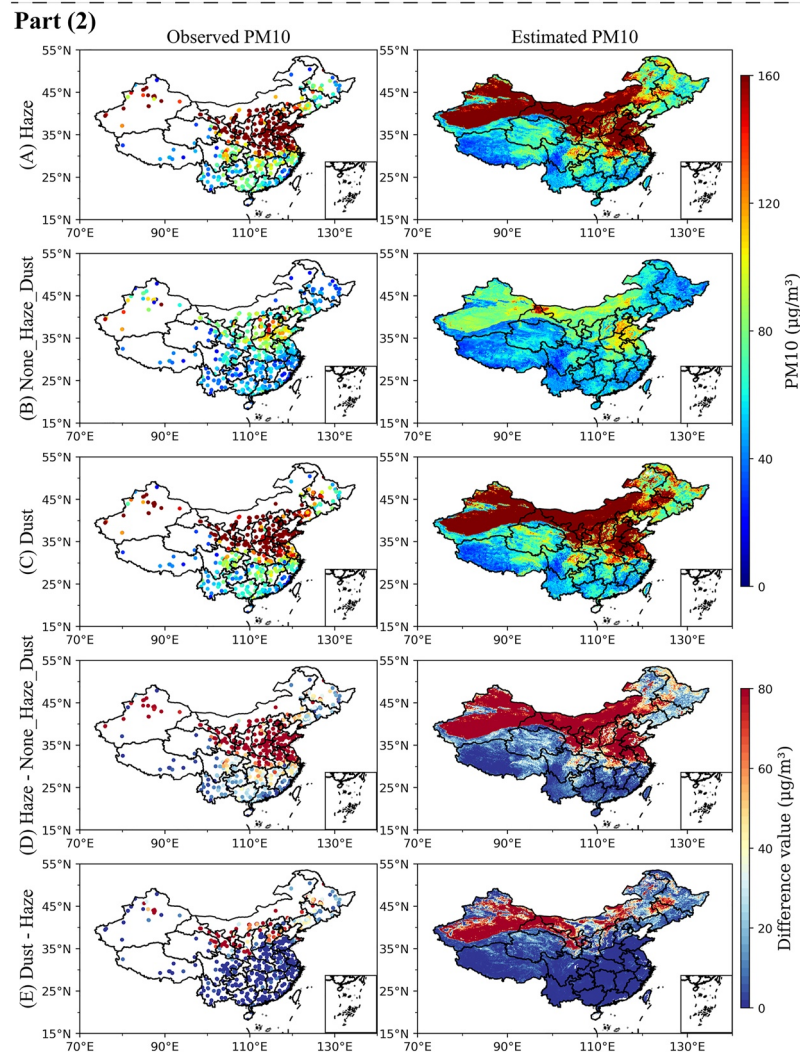
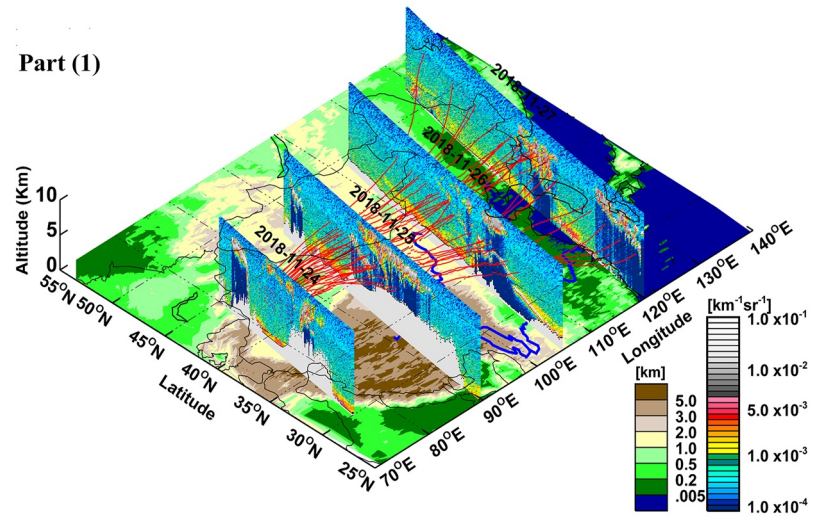


Figure 11. Identical Figure 9, Part I showed mixed pollution event of dust weather and haze weather (24–27 November 2018). And Figure line (a–e) showed the average atmospheric PM_{10} concentration during the Haze period (November 24–30), None_Haze_Dust period (November 1–23), Dust period (November 25–27), the difference between Haze period and None_Haze_Dust period, and difference between Dust period and Haze period, respectively.

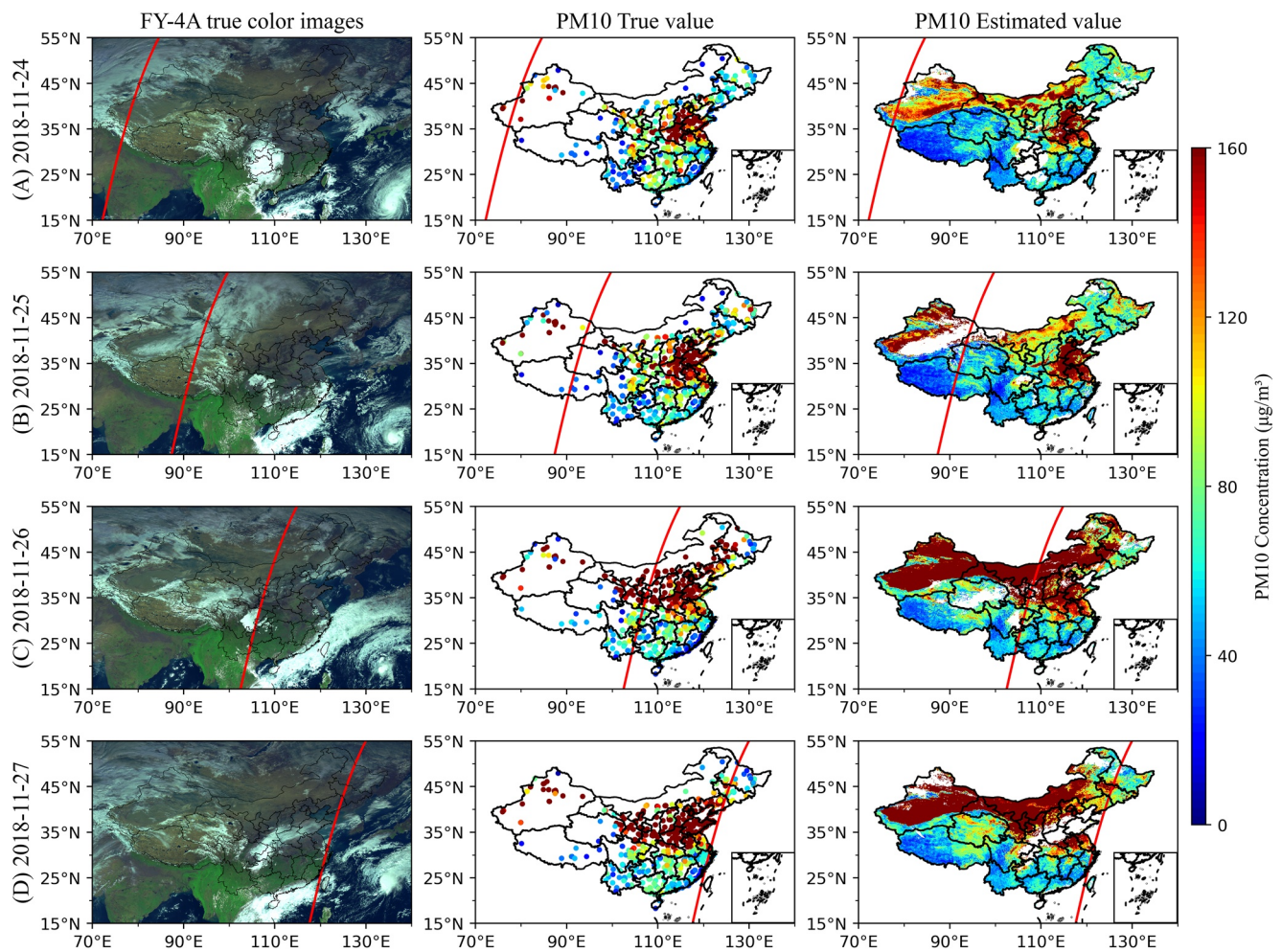


Figure 12. The same as Figure 10, except for 2018 [Line (a): 11–24, Line (b): 11–25, Line (c): 11–26, and Line (d): 11–27].

larger range of the dust weather observed on November 26 and the dust transmission path. On November 27, the wind speed in northern China decreased, and the dust weather ceased.

Figure 11 (Part 2) showed the atmospheric PM_{10} concentration distribution estimated by the model and observed by the station. The atmospheric PM_{10} concentration on haze days (Figure 11a, haze period) was much greater than that on the None_Haze_Dust days (Figure 11b), and the PM_{10} concentration on dust days (Figure 11c, dust period) was the greatest. The estimated and observed PM_{10} in Haze period were 122.60 and 146.42 $\mu\text{g}/\text{m}^3$ (northern China: 162.60 and 209.36 $\mu\text{g}/\text{m}^3$), respectively. During the dust period the values were 154.07 and 158.98 $\mu\text{g}/\text{m}^3$ (northern China: 214.62 and 257.31 $\mu\text{g}/\text{m}^3$), respectively. In November 2018, the estimated and observed atmospheric PM_{10} concentration in the None_Haze_Dust period were 62.28 and 65.37 $\mu\text{g}/\text{m}^3$ (northern China: 70.62 and 88.11 $\mu\text{g}/\text{m}^3$). There were two principal reasons why the estimated value of the model was less than the observed value of the station. A reason for this was the lack of data in some areas due to the existence of clouds. Second, the sample size of the model average was much larger than the number of stations on the station average.

Figure 11d showed the difference in atmospheric PM_{10} concentration between the haze period and the None_Haze_Dust period. Based on the model PM_{10} , during the haze period, the PM_{10} in 74% of China increased by 20%, 53% of China increased by 50%, 43% of China increased by 70%, 17% of China increased by 100%, and 10% of China increased by 200%. The observed atmospheric PM_{10} concentration increased by 20% at 1,327 stations (accounting for 83% of the total number of stations). That of 1,109 stations (69%) increased by 50%, that of 948 stations (59%) increased by 70%, that of 713 stations (44%) increased by 100%, and that of 204 stations

Table 3
Comparison of PM_{10} Model Performance in This Study With Earlier Studies

References	Model	Model performance			Instrument	Data	Region	Study period
		R^2	RMSE	MAE				
L. Chen et al. (2012)	Land use regression model	0.84	0.21	/	/	/	Tian-jin, China	2006
T. H. Zhang et al. (2016)	Geographically weighted regression	0.67	/	/	MODIS	AOD	China	2015
You et al. (2015)	Geographically weighted regression	0.77	16.91	/	MODIS	AOD	Xi'an, China	2011–2013
G. Chen et al. (2018)	Random forest	0.78	31.54	/	MODIS	AOD	China	2005–2016
Z. Zhang et al. (2018)	Land use regression model	0.64	/	/	MODIS	AOD	China	2014–2016
Stafoggia et al. (2019)	Random forest	0.75	/	/	MODIS	AOD	Italy	2013–2015
Hough et al. (2021)	Random forest	0.71	/	4.26	MODIS	AOD	France	2000–2019
Gupta et al. (2021)	Geographically weighted regression	0.72	/	/	INSAT-3D	AOD	India	2014–2018
S. Park et al. (2021)	Gradient boosted regression trees	0.82	34.9	/	GOCI	AOD	Korea	2019
Wei, Li, Xue, et al. (2021)	Space-time extremely randomized trees	0.86	24.28	14.52	MODIS	AOD	China	2015–2019
This study	Decision tree	0.38	43.32	23.22	AGRI	TOAR	China	2018–2019
This study	Random forest	0.71	29.59	16.61	AGRI	TOAR	China	2018–2019
This study	Extreme tree	0.74	28.02	15.51	AGRI	TOAR	China	2018–2019
This study	Deep forest	0.82	24.16	11.23	AGRI	TOAR	China	2018–2019

(13%) increased by 200%. Figure 11e showed the results of the atmospheric PM_{10} concentration comparison between the dust and haze periods, which one may estimate the contribution of LRTD to haze weather. Based on the model results, due to the LRTD transport of dust, atmospheric PM_{10} concentration increased by 20% in 33% and 50% in 11% of China. Based on surface station data, atmospheric PM_{10} concentration observations at 352 stations (22% of the total number of stations) increased by 20%, and that at 116 stations (7%) increased by 50%. As shown in Figure 11e, the dust weather mainly affected the PM_{10} concentration in the dust transmission path areas, such as China's Hexi Corridor and Inner Mongolia.

5. Conclusions

The hourly atmospheric PM_{10} concentrations in China were obtained using an interpretable deep learning model (DF model) and FY-4A TOAR data from June 2018 to May 2019. The main conclusions were as follows:

The optimal hourly R^2 of 10-fold cross validation of TOAR- PM_{10} DF model can reach 0.85 (13:00 Beijing time); The R^2 (RMSE) of daily, monthly, seasonal, and annual average were 0.82 (24.16 $\mu\text{g}/\text{m}^3$), 0.97 (6.53 $\mu\text{g}/\text{m}^3$), 0.98 (4.17 $\mu\text{g}/\text{m}^3$), and 0.99 (2.3 $\mu\text{g}/\text{m}^3$), respectively. The model performance (R^2 , RMSE) was better in the YRD (0.86 and 15.70 $\mu\text{g}/\text{m}^3$), BTH (0.86, 22.04 $\mu\text{g}/\text{m}^3$), and CC (0.87, 18.05 $\mu\text{g}/\text{m}^3$) region. The average PM_{10} concentrations in spring, summer, autumn, and winter in China were 67.90 ± 25.78 , 49.8 ± 20.06 , 58.68 ± 22.16 , and 73.46 ± 26.27 $\mu\text{g}/\text{m}^3$, respectively. In spring, the PM_{10} concentration in northern China was higher than that in southern China, which may be related to the LRTD (Tao et al., 2021; L. Zhao et al., 2020). Excluding the dust weather periods, the areas with high PM_{10} values in China were mainly in large cities and suburban areas, which were related to local human activities (Tao et al., 2014).

The DF model can obtain the importance of the model features. The results of the FY-4A TOAR- PM_{10} model showed that TOAR, BLH, RH, surface wind speed (U10 and V10), TM, and TIME contributed significantly to the model. The performance of the model was related to the contributions of these important features (Chen, Song, Shi, & Li, 2022). The performance of the model would be worse in areas with a large contribution to surface pressure (SP). As shown in Table 3, the performance of the FY-4A TOAR- PM_{10} model was better than that of other researchers using the AOD- PM_{10} model. Using the same FY-4A TOAR and other auxiliary data, the DF model performed better than other traditional machine learning models (such as DT, RF, and ET).

China's arid and semi-arid regions account for ~57% of the country's land (Y. Yang et al., 2019). The dust transmitted from these regions every year has an important impact on China's air pollutants (such as PM_{10}). Using

the results of the TOAR-PM₁₀ model, the contribution of LRTD to local atmospheric PM₁₀ concentrations was quantified. During the weather promoting dust disturbance and transport (14–17 May 2019), the contributions of LRTD to PM₁₀ in China and northern China were 30.07 (52.3%) and 52 (80.4%) μg/m³, respectively. When haze weather and dust weather were mixed (24–30 November 2018), the PM₁₀ concentrations in China and northern China increased by 60.32 (96.9%) and 91.98 (130.2%) μg/m³, respectively. Compared with PM₁₀ on haze days, PM₁₀ on dust days in China and northern China increased by 31.47 (50.5%) and 52.02 (73.7%) μg/m³, respectively. The results were similar to those of others (Chen, Song, Shi, & Li, 2022; Gobbi et al., 2013; Guan et al., 2019; Remoundaki et al., 2013). The source (originating from the Taklimakan Desert in China) and transmission path of the two dust weather processes were similar, and the contribution to atmospheric PM₁₀ concentration in China and northern China was the same, but the intensity of the second dust weather was weaker than that of the first dust weather. In other words, the contribution of LRTD to local PM₁₀ was not only related to the intensity of dust weather, but also to meteorological conditions such as ground wind speed (Dimitriou & Kassomenos, 2018; Gobbi et al., 2019). In the first dust weather, the ground wind speed was large, which was conducive to the diffusion of ground pollutants and the reduction of atmospheric PM₁₀ concentration; The second, the low wind speed was conducive to the dry settlement of dust and the increase of PM₁₀ concentration. The results showed that the contribution of LRTD and local pollution to PM₁₀ in haze days was both important.

Data Availability Statement

The PM₁₀ data were obtained from the China Environmental Monitoring Center, <http://www.cnemc.cn> (CEMC, 2022). The FY-4A TOAR data provided by the National Satellite Meteorological Center of China, <http://satellite.nsmc.org.cn/PortalSite/Data/Satellite.aspx> (NSMC, 2022). ERA5 meteorological data can be downloaded from the European Centre for Medium-Range Weather Forecasts, <https://cds.climate.copernicus.eu/cdsapp#!/dataset/reanalysis-era5-land> (ECMWF, 2022). The height data download from CGIAR Consortium for Spatial Information, <https://srtm.csi.cgiar.org/srtmdata/> (CCSI, 2022). Population density data provided by NASA's Socioeconomic Data and Applications Center, <http://sedac.ciesin.columbia.edu/data/collection/gpw-v4/documentation> (SEDAC, 2022). The estimated data and data reading codes are available from <https://doi.org/10.5281/zenodo.6459693>. All programs in this study are implemented based on Python3, <https://www.python.org/> (Python3, 2022).

Acknowledgments

The work Supported by the Second Tibetan Plateau Scientific Expedition and Research Program (STEP; Grant No. Grant number 2019QZKK0602), the National Key Research and Development Program of China (Grant No. Grant number 2019YFA0606800) and the National Natural Science Foundation of China (Grant 41775021). The authors would like to thank China National Environmental Monitoring Center, National Satellite Meteorological Center of China, and European Centre for Medium-Range Weather Forecasts and NASA for their datasets.

References

- Bai, H., Zheng, Z., Zhang, Y., Huang, H., & Wang, L. (2021). Comparison of satellite-based PM_{2.5} estimation from aerosol optical depth and top-of-atmosphere reflectance. *Aerosol and Air Quality Research*, 21, 200257. <https://doi.org/10.4209/aaqr.2020.05.0257>
- Breiman, L. (2001). Random forests. *Machine Learning*, 45, 5–32. <https://doi.org/10.1023/A:1010933404324>
- Brook, R. D., Rajagopalan, S., Pope, C. A., Brook, J. R., Bhatnagar, A., Diez-Roux, A. V., et al. (2010). Particulate matter air pollution and cardiovascular disease. *Circulation*, 121, 2331–2378. <https://doi.org/10.1161/CIR.0b013e3181d8bec1>
- CCSI. (2022). SRTM3. [Data set]. CCSI. Retrieved from <https://srtm.csi.cgiar.org/srtmdata/>
- CEMC. (2022). PM10. [Data set]. CEMC. Retrieved from <http://www.cnemc.cn>
- Chen, B., Huang, J., Minnis, P., Hu, Y., Yi, Y., Liu, Z., et al. (2010). Detection of dust aerosol by combining CALIPSO active lidar and passive IIR measurements. *Atmospheric Chemistry and Physics*, 10, 4241–4251. <https://doi.org/10.5194/acp-10-4241-2010>
- Chen, B., Song, Z., Pan, F., & Huang, Y. (2022). Obtaining vertical distribution of PM_{2.5} from CALIOP data and machine learning algorithms. *The Science of the Total Environment*, 805, 150338. <https://doi.org/10.1016/j.scitotenv.2021.150338>
- Chen, B., Song, Z., Shi, B., & Li, M. (2022). An interpretable deep forest model for estimating hourly PM10 concentration in China using Himawari-8 data. *Atmospheric Environment*, 268, 118827. <https://doi.org/10.1016/j.atmosenv.2021.118827>
- Chen, G., Wang, Y., Li, S., Cao, W., Ren, H., Knibbs, L. D., et al. (2018). Spatiotemporal patterns of PM10 concentrations over China during 2005–2016: A satellite-based estimation using the random forests approach. *Environmental Pollution*, 242, 605–613. <https://doi.org/10.1016/j.envpol.2018.07.012>
- Chen, J., Yin, J., Zang, L., Zhang, T., & Zhao, M. (2019). Stacking machine learning model for estimating hourly PM_{2.5} in China based on Himawari 8 aerosol optical depth data. *The Science of the Total Environment*, 697, 134021. <https://doi.org/10.1016/j.scitotenv.2019.134021>
- Chen, L., Wang, Y., Li, P., Ji, Y., Kong, S., Li, Z., et al. (2012). A land use regression model incorporating data on industrial point source pollution. *Journal of Environmental Sciences*, 24, 1251–1258. [https://doi.org/10.1016/S1001-0742\(11\)60902-9](https://doi.org/10.1016/S1001-0742(11)60902-9)
- Chen, M., Guo, S., Hu, M., & Zhang, X. (2020). The spatiotemporal evolution of population exposure to PM_{2.5} within the Beijing-Tianjin-Hebei urban agglomeration, China. *Journal of Cleaner Production*, 265, 121708. <https://doi.org/10.1016/j.jclepro.2020.121708>
- Chen, Y., Chen, G., Cui, C., Zhang, A., Wan, R., Zhou, S., et al. (2020). Retrieval of the vertical evolution of the cloud effective radius from the Chinese FY-4 (Feng Yun 4) next-generation geostationary satellites. *Atmospheric Chemistry and Physics*, 20, 1131–1145. <https://doi.org/10.5194/acp-20-1131-2020>
- China. (2012). *Ambient air quality standards. GB 3095-2012*. China Environmental Science Press.
- Chu, D. A., Kaufman, Y. J., Zibordi, G., Chern, J. D., Mao, J., Li, C., et al. (2003). Global monitoring of air pollution over land from the Earth observing system-terra Moderate Resolution Imaging Spectroradiometer (MODIS). *Journal of Geophysical Research*, 108. <https://doi.org/10.1029/2002JD003179>

- Dimitriou, K., & Kassomenos, P. (2018). Day by day evolution of a vigorous two wave Saharan dust storm - Thermal and air quality impacts. *Atmosfera*, 31, 105–124. <https://doi.org/10.20937/Atm.2018.31.02.01>
- ECMWF. (2022). ECMWF: ERA5 [Data set]. ECMWF. Retrieved from <https://cds.climate.copernicus.eu/cdsapp#!/dataset/reanalysis-era5-land>
- Fu, Q., Zhuang, G., Wang, J., Xu, C., Huang, K., Li, J., et al. (2008). Mechanism of formation of the heaviest pollution episode ever recorded in the Yangtze River Delta, China. *Atmospheric Environment*, 42, 2023–2036. <https://doi.org/10.1016/j.atmosenv.2007.12.002>
- Gao, M., Carmichael, G. R., Wang, Y., Saide, P. E., Yu, M., Xin, J., et al. (2016). Modeling study of the 2010 regional haze event in the North China Plain. *Atmospheric Chemistry and Physics*, 16, 1673–1691. <https://doi.org/10.5194/acp-16-1673-2016>
- Geurts, P., Ernst, D., & Wehenkel, L. (2006). Extremely randomized trees. *Machine Learning*, 63, 3–42. <https://doi.org/10.1007/s10994-006-6226-1>
- Gobbi, G. P., Angelini, F., Barnaba, F., Costabile, F., Baldasano, J. M., Basart, S., et al. (2013). Changes in particulate matter physical properties during Saharan advections over Rome (Italy): A four-year study, 2001–2004. *Atmospheric Chemistry and Physics*, 13, 7395–7404. <https://doi.org/10.5194/acp-13-7395-2013>
- Gobbi, G. P., Barnaba, F., Di Liberto, L., Bolignano, A., Lucarelli, F., Nava, S., et al. (2019). An inclusive view of Saharan dust advections to Italy and the Central Mediterranean. *Atmospheric Environment*, 201, 242–256. <https://doi.org/10.1016/j.atmosenv.2019.01.002>
- Guan, Q., Luo, H., Pan, N., Zhao, R., Yang, L., Yang, Y., et al. (2019). Contribution of dust in northern China to PM10 concentrations over the Hexi corridor. *The Science of the Total Environment*, 660, 947–958. <https://doi.org/10.1016/j.scitotenv.2018.12.412>
- Gui, K., Che, H., Zeng, Z., Wang, Y., Zhai, S., Wang, Z., et al. (2020). Construction of a virtual PM2.5 observation network in China based on high-density surface meteorological observations using the Extreme Gradient Boosting model. *Environment International*, 141, 105801. <https://doi.org/10.1016/j.envint.2020.105801>
- Guo, J.-P., Zhang, X.-Y., Che, H.-Z., Gong, S.-L., An, X., Cao, C.-X., et al. (2009). Correlation between PM concentrations and aerosol optical depth in eastern China. *Atmospheric Environment*, 43, 5876–5886. <https://doi.org/10.1016/j.atmosenv.2009.08.026>
- Gupta, A., Kant, Y., Mitra, D., & Chauhan, P. (2021). Spatio-temporal distribution of INSAT-3D AOD derived particulate matter concentration over India. *Atmospheric Pollution Research*, 12, 159–172. <https://doi.org/10.1016/j.apr.2020.08.031>
- Han, S., Liu, J., Hao, T., Zhang, Y., Li, P., Yang, J., et al. (2018). Boundary layer structure and scavenging effect during a typical winter haze-fog episode in a core city of BTH region, China. *Atmospheric Environment*, 179, 187–200. <https://doi.org/10.1016/j.atmosenv.2018.02.023>
- Ho, H. C., Wong, M. S., Yang, L., Shi, W., Yang, J., Bilal, M., et al. (2018). Spatiotemporal influence of temperature, air quality, and urban environment on cause-specific mortality during hazy days. *Environment International*, 112, 10–22. <https://doi.org/10.1016/j.envint.2017.12.001>
- Hough, I., Sarafian, R., Shtein, A., Zhou, B., Lepeule, J., & Kloog, I. (2021). Gaussian Markov random fields improve ensemble predictions of daily 1 km PM2.5 and PM10 across France. *Atmospheric Environment*, 264, 118693. <https://doi.org/10.1016/j.atmosenv.2021.118693>
- Hu, X., Waller, L. A., Lyapustin, A., Wang, Y., Al-Hamdan, M. Z., Crosson, W. L., et al. (2014). Estimating ground-level PM2.5 concentrations in the Southeastern United States using MAIAC AOD retrievals and a two-stage model. *Remote Sensing of Environment*, 140, 220–232. <https://doi.org/10.1016/j.rse.2013.08.032>
- Jiang, J., Zhou, W., Cheng, Z., Wang, S., He, K., & Hao, J. (2015). Particulate matter distributions in China during a winter period with frequent pollution episodes (January 2013). *Aerosol and Air Quality Research*, 15, 494–503. <https://doi.org/10.4209/aaqr.2014.04.0070>
- Kanniah, K. D., Nurul Amalin Fatimah Kamarul, Z., Lim, H. Q., & Mohd Nadzri, M. R. (2014). Monitoring particulate matters in urban areas in Malaysia using remote sensing and ground-based measurements. *Proceedings of SPIE*, 9242. <https://doi.org/10.1117/12.2067029>
- Kassomenos, P. A., Vardoulakis, S., Chaloulakou, A., Paschalidou, A. K., Grivas, G., Borge, R., et al. (2014). Study of PM10 and PM2.5 levels in three European cities: Analysis of intra and inter urban variations. *Atmospheric Environment*, 87, 153–163. <https://doi.org/10.1016/j.atmosenv.2014.01.004>
- Ke, G. L., Meng, Q., Finley, T., Wang, T. F., Chen, W., Ma, W. D., et al. (2017). LightGBM: A highly efficient gradient boosting decision tree. *Advances in Neural Information Processing Systems*, 30, 30.
- Kloog, I., Sorek-Hamer, M., Lyapustin, A., Coull, B., Wang, Y., Just, A. C., et al. (2015). Estimating daily PM2.5 and PM10 across the complex geo-climate region of Israel using MAIAC satellite-based AOD data. *Atmospheric Environment*, 122, 409–416. <https://doi.org/10.1016/j.atmosenv.2015.10.004>
- Li, T., Shen, H., Yuan, Q., Zhang, X., & Zhang, L. (2017). Estimating ground-level PM2.5 by fusing satellite and station observations: A geo-intelligent deep learning approach. *Geophysical Research Letters*, 44(11), 985–993. <https://doi.org/10.1002/2017GL075710>
- Li, Z., Zhang, Y., Shao, J., Li, B., Hong, J., Liu, D., et al. (2016). Remote sensing of atmospheric particulate mass of dry PM2.5 near the ground: Method validation using ground-based measurements. *Remote Sensing of Environment*, 173, 59–68. <https://doi.org/10.1016/j.rse.2015.11.019>
- Liu, F., Tan, Q., Jiang, X., Yang, F., & Jiang, W. (2019). Effects of relative humidity and PM2.5 chemical compositions on visibility impairment in Chengdu, China. *Journal of Environmental Sciences*, 86, 15–23. <https://doi.org/10.1016/j.jes.2019.05.004>
- Liu, J., Weng, F., & Li, Z. (2019). Satellite-based PM2.5 estimation directly from reflectance at the top of the atmosphere using a machine learning algorithm. *Atmospheric Environment*, 208, 113–122. <https://doi.org/10.1016/j.atmosenv.2019.04.002>
- Ma, S., Shao, M., Zhang, Y., Dai, Q., & Xie, M. (2021). Sensitivity of PM2.5 and O3 pollution episodes to meteorological factors over the North China Plain. *The Science of the Total Environment*, 792, 148474. <https://doi.org/10.1016/j.scitotenv.2021.148474>
- Mao, F., Hong, J., Min, Q., Gong, W., Zang, L., & Yin, J. (2021). Estimating hourly full-coverage PM2.5 over China based on TOA reflectance data from the Fengyun-4A satellite. *Environmental Pollution*, 270, 116119. <https://doi.org/10.1016/j.envpol.2020.116119>
- Meng, C., & Li, H. (2019). Assimilating satellite land surface states data from Fengyun-4A. *Scientific Reports*, 9, 19567. <https://doi.org/10.1038/s41598-019-55733-3>
- Meng, X., Garay, M. J., Diner, D. J., Kalashnikova, O. V., Xu, J., & Liu, Y. (2018). Estimating PM2.5 speciation concentrations using prototype 4.4 km-resolution MISR aerosol properties over Southern California. *Atmospheric Environment*, 181, 70–81. <https://doi.org/10.1016/j.atmosenv.2018.03.019>
- Millán-Martínez, M., Sánchez-Rodas, D., Sánchez dela Campa, A. M., & Dela Rosa, J. (2021). Contribution of anthropogenic and natural sources in PM10 during North African dust events in Southern Europe. *Environmental Pollution*, 290, 118065. <https://doi.org/10.1016/j.envpol.2021.118065>
- Min, M., Wu, C., Li, C., Liu, H., Xu, N., Wu, X., et al. (2017). Developing the science product algorithm testbed for Chinese next-generation geostationary meteorological satellites: Fengyun-4 series. *Journal of Meteorological Research*, 31, 708–719. <https://doi.org/10.1007/s13351-017-6161-z>
- NSMC. (2022). NSMC, FY-4A TOAR. [Data set]. NSMC. Retrieved from <http://satellite.nsmc.org.cn/PortalSite/Data/Satellite.aspx>
- Park, S., Kim, M., & Im, J. (2021). Estimation of ground-level PM10 and PM2.5 concentrations using boosting-based machine learning from satellite and Numerical weather Prediction data. *Korean Journal of Remote Sensing*, 37, 321–335. <https://doi.org/10.7780/kjrs.2021.37.2.11>
- Park, Y., Kwon, B., Heo, J., Hu, X., Liu, Y., & Moon, T. (2020). Estimating PM2.5 concentration of the conterminous United States via interpretable convolutional neural networks. *Environmental Pollution*, 256, 113395. <https://doi.org/10.1016/j.envpol.2019.113395>

- Paschalidou, A. K., Karakitsios, S., Kleanthous, S., & Kassomenos, P. A. (2011). Forecasting hourly PM10 concentration in Cyprus through artificial neural networks and multiple regression models: Implications to local environmental management. *Environmental Science and Pollution Research*, *18*, 316–327. <https://doi.org/10.1007/s11356-010-0375-2>
- Python3. (2022). Software. Retrieved from <https://www.python.org/>
- Qin, K., Zou, J., Guo, J., Lu, M., Bilal, M., Zhang, K., et al. (2018). Estimating PM1 concentrations from MODIS over Yangtze River Delta of China during 2014–2017. *Atmospheric Environment*, *195*, 149–158. <https://doi.org/10.1016/j.atmosenv.2018.09.054>
- Rastogi, N., Agnihotri, R., Sawlani, R., Patel, A., Babu, S. S., & Satish, R. (2020). Chemical and isotopic characteristics of PM10 over the Bay of Bengal: Effects of continental outflow on a marine environment. *The Science of the Total Environment*, *726*, 138438. <https://doi.org/10.1016/j.scitotenv.2020.138438>
- Remoundaki, E., Papayannis, A., Kassomenos, P., Mantas, E., Kokkalis, P., & Tsezos, M. (2013). Influence of Saharan dust transport events on PM2.5 concentrations and composition over Athens. *Water, Air, & Soil Pollution*, *224*, 1373. <https://doi.org/10.1007/s11270-012-1373-4>
- Rodriguez, J. D., Perez, A., & Lozano, J. A. (2010). Sensitivity analysis of k-fold cross validation in prediction error estimation. *IEEE Transactions on Pattern Analysis and Machine Intelligence*, *32*, 569–575. <https://doi.org/10.1109/TPAMI.2009.187>
- Samoli, E., Kougea, E., Kassomenos, P., Analitis, A., & Katsouyanni, K. (2011). Does the presence of desert dust modify the effect of PM10 on mortality in Athens, Greece? *The Science of the Total Environment*, *409*, 2049–2054. <https://doi.org/10.1016/j.scitotenv.2011.02.031>
- SEDAC. (2022). SEDAC, Gridded Population of the World (GPW). [Data set]. SEDAC. Retrieved from <http://sedac.ciesin.columbia.edu/data/collection/gpw-v4/documentationdataset>
- Song, Z., Chen, B., Huang, Y., Dong, L., & Yang, T. (2021). Estimation of PM2.5 concentration in China using linear hybrid machine learning model. *Atmospheric Measurement Techniques*, *14*, 5333–5347. <https://doi.org/10.5194/amt-14-5333-2021>
- Stafoggia, M., Bellander, T., Bucci, S., Davoli, M., deHoogh, K., de' Donato, F., et al. (2019). Estimation of daily PM10 and PM2.5 concentrations in Italy, 2013–2015, using a spatiotemporal land-use random-forest model. *Environment International*, *124*, 170–179. <https://doi.org/10.1016/j.envint.2019.01.016>
- Sun, L., Wei, J., Duan, D. H., Guo, Y. M., Yang, D. X., Jia, C., et al. (2016). Impact of Land-Use and Land-Cover Change on urban air quality in representative cities of China. *Journal of Atmospheric and Solar-Terrestrial Physics*, *142*, 43–54. <https://doi.org/10.1016/j.jastp.2016.02.022>
- Tao, M., Chen, L., Wang, Z., Ma, P., Tao, J., & Jia, S. (2014). A study of urban pollution and haze clouds over northern China during the dusty season based on satellite and surface observations. *Atmospheric Environment*, *82*, 183–192. <https://doi.org/10.1016/j.atmosenv.2013.10.010>
- Tao, M., Gui, L., Li, R., Wang, L., Liang, S., Li, Q., et al. (2021). Tracking prevailing dust aerosol over the air pollution in central China with integrated satellite and ground observations. *Atmospheric Environment*, *253*, 118369. <https://doi.org/10.1016/j.atmosenv.2021.118369>
- Tomczak, A., Miller, A. B., Weichenthal, S. A., To, T., Wall, C., vanDonkelaar, A., et al. (2016). Long-term exposure to fine particulate matter air pollution and the risk of lung cancer among participants of the Canadian National Breast Screening Study. *International Journal of Cancer*, *139*, 1958–1966. <https://doi.org/10.1002/ijc.30255>
- Wang, W., Mao, F., Du, L., Pan, Z., Gong, W., & Fang, S. (2017). Deriving hourly PM2.5 concentrations from himawari-8 AODs over Beijing–Tianjin–Hebei in China. *Remote Sensing*, *9*, 858. <https://doi.org/10.3390/rs9080858>
- Wang, X., Sun, W., Zheng, K., Ren, X., & Han, P. (2020). Estimating hourly PM2.5 concentrations using MODIS 3 km AOD and an improved spatiotemporal model over Beijing–Tianjin–Hebei, China. *Atmospheric Environment*, *222*, 117089. <https://doi.org/10.1016/j.atmosenv.2019.117089>
- Wei, J., Huang, W., Li, Z., Xue, W., Peng, Y., Sun, L., et al. (2019). Estimating 1-km-resolution PM2.5 concentrations across China using the space-time random forest approach. *Remote Sensing of Environment*, *231*, 111221. <https://doi.org/10.1016/j.rse.2019.111221>
- Wei, J., Li, Z., Pinker, R. T., Wang, J., Sun, L., Xue, W., et al. (2021). Himawari-8-derived diurnal variations in ground-level PM2.5 pollution across China using the fast space-time Light Gradient Boosting Machine (LightGBM). *Atmospheric Chemistry and Physics*, *21*, 7863–7880. <https://doi.org/10.5194/acp-21-7863-2021>
- Wei, J., Li, Z., Xue, W., Sun, L., Fan, T., Liu, L., et al. (2021). The ChinaHighPM10 dataset: Generation, validation, and spatiotemporal variations from 2015 to 2019 across China. *Environment International*, *146*, 106290. <https://doi.org/10.1016/j.envint.2020.106290>
- Wu, J., Yao, F., Li, W., & Si, M. (2016). VIIRS-based remote sensing estimation of ground-level PM2.5 concentrations in Beijing–Tianjin–Hebei: A spatiotemporal statistical model. *Remote Sensing of Environment*, *184*, 316–328. <https://doi.org/10.1016/j.rse.2016.07.015>
- Xia, X., Min, J., Shen, F., Wang, Y., Xu, D., Yang, C., et al. (2020). Aerosol data assimilation using data from Fengyun-4A, a next-generation geostationary meteorological satellite. *Atmospheric Environment*, *237*, 117695. <https://doi.org/10.1016/j.atmosenv.2020.117695>
- Xiao, Q., Ma, Z., Li, S., & Liu, Y. (2015). The impact of winter heating on air pollution in China. *PLoS One*, *10*, e0117311. <https://doi.org/10.1371/journal.pone.0117311>
- Xiong, H.-B., Chen, J., Ma, X., & Fang, M.-Y. (2021). Estimating the PM2.5 concentration over Anhui Province, China, using the himawari-8 AOD and a GAM/BME model. *Atmospheric Pollution Research*, *12*, 101110. <https://doi.org/10.1016/j.apr.2021.101110>
- Xu, B., Lin, W., & Taqi, S. A. (2020). The impact of wind and non-wind factors on PM2.5 levels. *Technological Forecasting and Social Change*, *154*, 119960. <https://doi.org/10.1016/j.techfore.2020.119960>
- Xu, G., Ren, X., Xiong, K., Li, L., Bi, X., & Wu, Q. (2020). Analysis of the driving factors of PM2.5 concentration in the air: A case study of the Yangtze River Delta, China. *Ecological Indicators*, *110*, 105889. <https://doi.org/10.1016/j.ecolind.2019.105889>
- Xu, Q., Chen, X., Yang, S., Tang, L., & Dong, J. (2021). Spatiotemporal relationship between Himawari-8 hourly columnar aerosol optical depth (AOD) and ground-level PM2.5 mass concentration in mainland China. *The Science of the Total Environment*, *765*, 144241. <https://doi.org/10.1016/j.scitotenv.2020.144241>
- Yan, X., Zang, Z., Luo, N., Jiang, Y., & Li, Z. (2020). New interpretable deep learning model to monitor real-time PM2.5 concentrations from satellite data. *Environment International*, *144*, 106060. <https://doi.org/10.1016/j.envint.2020.106060>
- Yang, J., Zhang, Z., Wei, C., Lu, F., & Guo, Q. (2017). Introducing the new generation of Chinese geostationary weather satellites, Fengyun-4. *Bulletin of the American Meteorological Society*, *98*, 1637–1658. <https://doi.org/10.1175/BAMS-D-16-0065.1>
- Yang, L., Xu, H., & Yu, S. (2020). Estimating PM2.5 concentrations in Yangtze River Delta region of China using random forest model and the Top-of-Atmosphere reflectance. *Journal of Environmental Management*, *272*, 111061. <https://doi.org/10.1016/j.jenvman.2020.111061>
- Yang, X., Zhao, C., Luo, N., Zhao, W., Shi, W., & Yan, X. (2020). Evaluation and Comparison of Himawari-8 L2 V1.0, V2.1 and MODIS C6.1 aerosol products over Asia and the Oceania regions. *Atmospheric Environment*, *220*, 117068. <https://doi.org/10.1016/j.atmosenv.2019.117068>
- Yang, Y., Bai, L., Wang, B., Wu, J., & Fu, S. (2019). Reliability of the global climate models during 1961–1999 in arid and semiarid regions of China. *The Science of the Total Environment*, *667*, 271–286. <https://doi.org/10.1016/j.scitotenv.2019.02.188>
- Yang, Y., Liao, H., & Lou, S. (2016). Increase in winter haze over eastern China in recent decades: Roles of variations in meteorological parameters and anthropogenic emissions. *Journal of Geophysical Research: Atmospheres*, *121*, 13050–13065. <https://doi.org/10.1002/2016JD025136>
- Yin, J., Mao, F., Zang, L., Chen, J., Lu, X., & Hong, J. (2021). Retrieving PM2.5 with high spatio-temporal coverage by TOA reflectance of Himawari-8. *Atmospheric Pollution Research*, *12*, 14–20. <https://doi.org/10.1016/j.apr.2021.02.007>

- You, W., Zang, Z., Zhang, L., Li, Z., Chen, D., & Zhang, G. (2015). Estimating ground-level PM10 concentration in northwestern China using geographically weighted regression based on satellite AOD combined with CALIPSO and MODIS fire count. *Remote Sensing of Environment*, 168, 276–285. <https://doi.org/10.1016/j.rse.2015.07.020>
- Zang, L., Mao, F., Guo, J., Wang, W., Pan, Z., Shen, H., et al. (2019). Estimation of spatiotemporal PM1.0 distributions in China by combining PM2.5 observations with satellite aerosol optical depth. *The Science of the Total Environment*, 658, 1256–1264. <https://doi.org/10.1016/j.scitotenv.2018.12.297>
- Zhang, P., Lu, Q., Hu, X., Gu, S., Yang, L., Min, M., et al. (2019). Latest progress of the Chinese meteorological satellite program and core data processing technologies. *Advances in Atmospheric Sciences*, 36, 1027–1045. <https://doi.org/10.1007/s00376-019-8215-x>
- Zhang, P., Zhu, L., Tang, S., Gao, L., Chen, L., Zheng, W., et al. (2019). General comparison of FY-4A/AGRI with other GEO/LEO instruments and its potential and challenges in non-meteorological Applications. *Frontiers of Earth Science*, 6, 224. <https://doi.org/10.3389/feart.2018.00224>
- Zhang, Q., Jiang, X., Tong, D., Davis, S. J., Zhao, H., Geng, G., et al. (2017). Transboundary health impacts of transported global air pollution and international trade. *Nature*, 543, 705–709. <https://doi.org/10.1038/nature21712>
- Zhang, Q., Zheng, Y., Tong, D., Shao, M., Wang, S., Zhang, Y., et al. (2019). Drivers of improved PM2.5 air quality in China from 2013 to 2017. *Proceedings of the National Academy of Sciences of the United States of America*, 116, 24463. <https://doi.org/10.1073/pnas.1907956116>
- Zhang, T., Zang, L., Wan, Y., Wang, W., & Zhang, Y. (2019). Ground-level PM2.5 estimation over urban agglomerations in China with high spatio-temporal resolution based on Himawari-8. *The Science of the Total Environment*, 676, 535–544. <https://doi.org/10.1016/j.scitotenv.2019.04.299>
- Zhang, T. H., Gong, W., Zhu, Z. M., Sun, K., Huang, Y. S., & Ji, Y. X. (2016). Semi-physical estimates of national-scale PM10 concentrations in China using a satellite-based geographically weighted regression model. *Atmosphere*, 7, 88. <https://doi.org/10.3390/atmos7070088>
- Zhang, X., Wang, F., Wang, W., Huang, F., Chen, B., Gao, L., et al. (2020). The development and application of satellite remote sensing for atmospheric compositions in China. *Atmospheric Research*, 245, 105056. <https://doi.org/10.1016/j.atmosres.2020.105056>
- Zhang, Y., & Li, Z. (2015). Remote sensing of atmospheric fine particulate matter (PM2.5) mass concentration near the ground from satellite observation. *Remote Sensing of Environment*, 160, 252–262. <https://doi.org/10.1016/j.rse.2015.02.005>
- Zhang, Y., Li, Z., Bai, K., Wei, Y., Xie, Y., Zhang, Y., et al. (2021). Satellite remote sensing of atmospheric particulate matter mass concentration: Advances, challenges, and perspectives. *Fundamental Research*, 1, 240–258. <https://doi.org/10.1016/j.fmre.2021.04.007>
- Zhang, Z., Wang, J., Hart, J. E., Laden, F., Zhao, C., Li, T., et al. (2018). National scale spatiotemporal land-use regression model for PM2.5, PM10 and NO2 concentration in China. *Atmospheric Environment*, 192, 48–54. <https://doi.org/10.1016/j.atmosenv.2018.08.046>
- Zhang, Z., Wu, W., Fan, M., Tao, M., Wei, J., Jin, J., et al. (2019). Validation of Himawari-8 aerosol optical depth retrievals over China. *Atmospheric Environment*, 199, 32–44. <https://doi.org/10.1016/j.atmosenv.2018.11.024>
- Zhao, C., & Garrett, T. J. (2015). Effects of Arctic haze on surface cloud radiative forcing. *Geophysical Research Letters*, 42, 557–564. <https://doi.org/10.1002/2014GL062015>
- Zhao, C., Wang, Q., Ban, J., Liu, Z., Zhang, Y., Ma, R., et al. (2020). Estimating the daily PM2.5 concentration in the Beijing-Tianjin-Hebei region using a random forest model with a 0.01° × 0.01° spatial resolution. *Environment International*, 134, 105297. <https://doi.org/10.1016/j.envint.2019.105297>
- Zhao, L., Wang, W., Hao, T., Qu, W., Sheng, L., Luo, C., et al. (2020). The autumn haze-fog episode enhanced by the transport of dust aerosols in the Tianjin area. *Atmospheric Environment*, 237, 117669. <https://doi.org/10.1016/j.atmosenv.2020.117669>
- Zhou, Z.-H., & Feng, J. (2017). Deep forest: Towards an alternative to deep neural networks. *Paper presented at the Proceedings of the Twenty-Sixth International Joint Conference on Artificial Intelligence Main track* (pp. 3553–3559). IJCAI. <https://doi.org/10.24963/ijcai.2017/497>